# Architecture of the cerebral cortical association connectome underlying cognition

Mihail Bota[a,1], Olaf Sporns[b], and Larry W. Swanson[a,2]

[a]Department of Biological Sciences, University of Southern California, Los Angeles, CA 90089; and [b]Department of Psychological and Brain Sciences, Indiana University, Bloomington, IN 47405

Contributed by Larry W. Swanson, March 9, 2015 (sent for review January 13, 2015; reviewed by Fred H. Gage and Marcus E. Raichle)

**Cognition presumably emerges from neural activity in the network of association connections between cortical regions that is modulated by inputs from sensory and state systems and directs voluntary behavior by outputs to the motor system. To reveal global architectural features of the cortical association connectome, network analysis was performed on >16,000 reports of histologically defined axonal connections between cortical regions in rat. The network analysis reveals an organization into four asymmetrically interconnected modules involving the entire cortex in a topographic and topologic core–shell arrangement. There is also a topographically continuous U-shaped band of cortical areas that are highly connected with each other as well as with the rest of the cortex extending through all four modules, with the temporal pole of this band (entorhinal area) having the most cortical association connections of all. These results provide a starting point for compiling a mammalian nervous system connectome that could ultimately reveal novel correlations between genome-wide association studies and connectome-wide association studies, leading to new insights into the cellular architecture supporting cognition.**

cerebral cortex | connectomics | mammal | network analysis | neural connections

The cerebral cortex is the core of the brain's cognitive system (1, 2). Emerging evidence suggests that misdirected and/or dysfunctional cortical connections established during neurodevelopment, or degenerative events later in life, are fundamental to cognitive alterations associated with brain disorders like Alzheimer's disease, autism spectrum disorder, and schizophrenia (3). Presumably, an understanding of biological mechanisms underlying cognition and the control of voluntary behavior rests at least partly on the structure–function wiring diagram of the cortex. Design principles of this neural circuitry are based on a network of interactions between distributed nervous system regions, and on the underlying function of their constituent neuron populations, and individual neurons.

Unfortunately, a global structure–function wiring diagram of the cortex has not yet been elaborated (4). A necessary, but not sufficient, prerequisite for establishing this basic plan is a comprehensive structural model of cortical connectivity (5–7). Such a "roadmap" could then be used as a database scaffolding for molecular, cellular, physiological, behavioral, and cognitive data and for modeling (8)—analogous to a Google Maps for the brain. The research strategy described here provides the starting point for such a model, as well as a framework, benchmark, and infrastructure for developing a global account of nervous system structural network organization as a whole.

The conceptual framework underlying our strategy to analyze global nervous system connection architecture is twofold. First, because of considerable complexity—for example, human isocortex on one side has 6–9 billion neurons (9–11) interconnected by orders-of-magnitude-more synapses—three hierarchical (nested) levels analysis are considered (12, 13). A macroconnection between two gray-matter regions considered as black boxes is at the top of the hierarchy, a mesoconnection between two neuron types (14) within or between regions is nested within a macroconnection, and a microconnection between two individual neurons anywhere in the nervous system is nested within a mesoconnection. Second, small mammals, instead of humans, are analyzed. Data are generated much more quickly from small brains, and experimental pathway tracing of human axonal connections is currently impermissible.

MR diffusion tractography offers exciting new approaches to identifying human cortical connections, but inherent resolution limits require correlation and validation with experimental histological pathway tracing data in animals. Tractography deals only with white-matter organization, not the cellular origin and synaptic termination of connections in gray matter, and the method cannot identify unambiguously the directionality (from–to relations) of identified tracts or distinguish histologically defined gray-matter regions themselves. Historically, similar limitations applied to the gross anatomical methods used to discover human regionalization and cortical association tracts almost 150 y ago (15).

Because the richest current experimental histological data on intracortical connectivity are for adult rat, this peer-reviewed neuroanatomical literature was systematically and expertly curated for network analysis. One goal was to begin by establishing a general plan for mammalian cortical association connections

## Significance

**Connections between cerebral cortex regions are known as association connections, and neural activity in the network formed by these connections is thought to generate cognition. Network analysis of microscopic association connection data produced over the last 40 years in a small, easily studied mammal suggests a new way to describe the organization of the cortical association network. Basically, it consists of four modules with an anatomical shell–core arrangement and asymmetric connections within and between modules, implying at least partly "hardwired," genetically determined biases of information flow through the cortical association network. The results advance the goal of achieving a global nervous system wiring diagram of connections and provide another step toward understanding the cellular architecture and mechanisms underpinning cognition.**

Author contributions: M.B. and L.W.S. designed research; M.B. performed research; M.B. and O.S. analyzed data; and L.W.S. wrote the paper.

Reviewers: F.H.G., The Salk Institute for Biological Studies; and M.E.R., Washington University in St. Louis.

The authors declare no conflict of interest.

Data deposition: The connectional data are available online at the Brain Architecture Knowledge Management System (BAMS; brancusi1.usc.edu/connections/grid/168); network analysis tools are available at the Brain Connectivity Toolbox (www.brain-connectivity-toolbox.net).

[1]Present address: International Neuroinformatics Coordinating Facility, University of California at San Diego, La Jolla, CA 92093.

[2]To whom correspondence should be addressed. Email: lswanson@usc.edu.

This article contains supporting information online at www.pnas.org/lookup/suppl/doi:10.1073/pnas.1504394112/-/DCSupplemental.

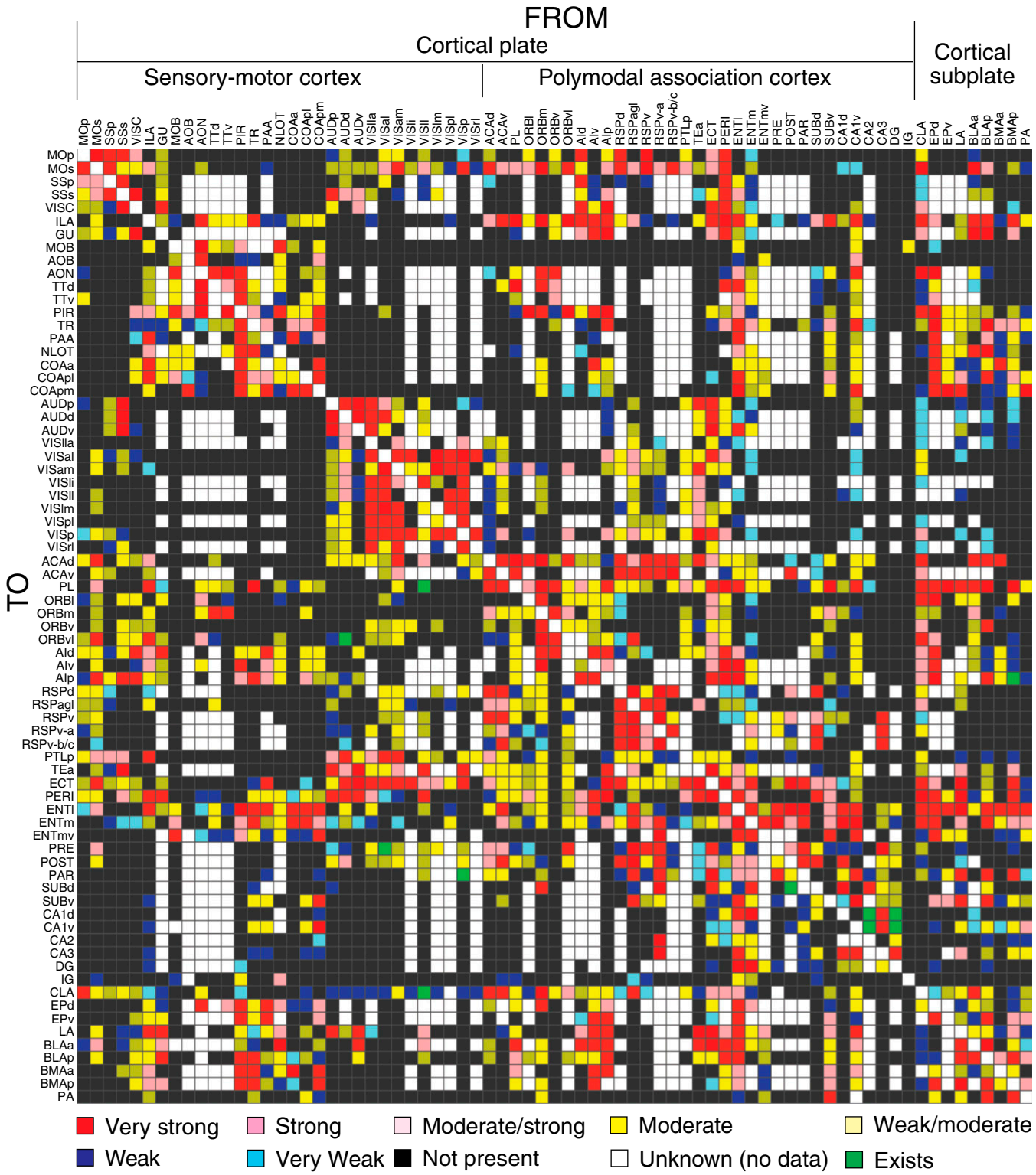


**Fig. 1.** Rat cortical association connectome. Directed synaptic macroconnection matrix with gray-matter region sequence (top left to right, list of macroconnection origins, from; left side top to bottom, same list of macroconnection terminations, to) in the Swanson-04 (16) structure–function nomenclature hierarchy. The main diagonal (top left to bottom right) is empty because connections within a region are not considered in the analysis. Color scale of connection weight is at bottom; abbreviations are in Fig. S2.

(4): excitatory (glutamatergic) connections established between cortical regions in one hemisphere by pyramidal neurons, as opposed to commissural connections between right and left hemispheres (a logical next step, followed by axonal inputs and outputs of the cortex). The other goal was to propose a comprehensive and systematic correlative bridge between data from experimental pathway tracing in animals and diffusion tractography in humans.

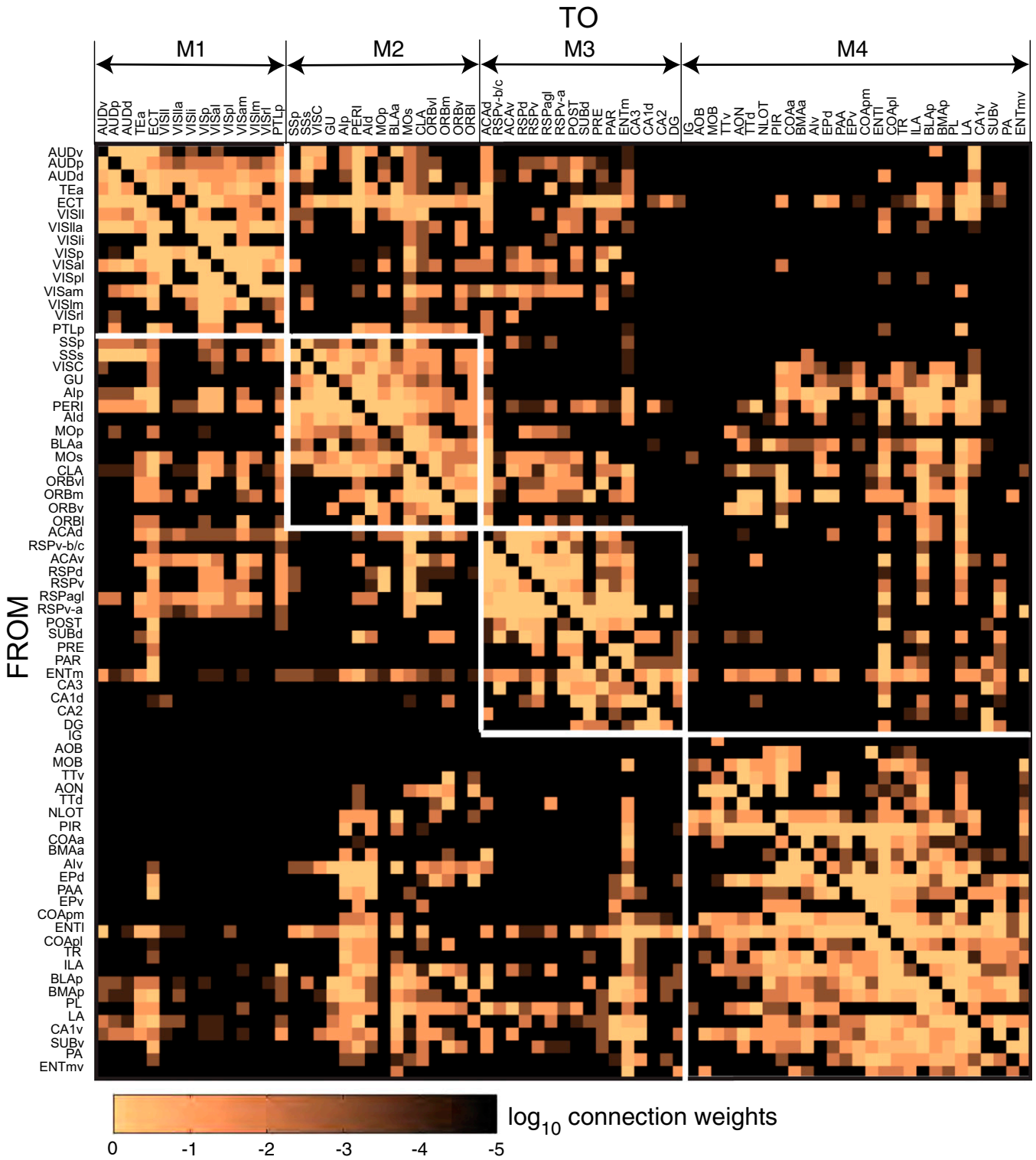


**Fig. 2.** Four modules of rat cortical association network (M1–M4). Directed synaptic macroconnections are arranged here by connection weight, rather than by nomenclature hierarchy (Fig. 1). The matrix (log-weighted scaled connection weighs, bottom) shows four highly interconnected modules (inside white boxes along main diagonal) that together include all 73 regions in the analysis, with intermodular connections shown outside the boxes. "Not present" and "unknown" are black; abbreviations are in Fig. S2.

## Results

**Cortical Association Connection Number.** Systematic curation of the primary neuroanatomical literature yielded 1,923 rat cortical association macroconnections (RCAMs) as present (242, or 12.6% from the L.W.S. laboratory) and 2,341 as not present (of those possible, 45.1% present, indicating a very highly connected network)—between the 73 gray-matter regions analyzed for the cerebral cortex as a whole. No adequate published data were

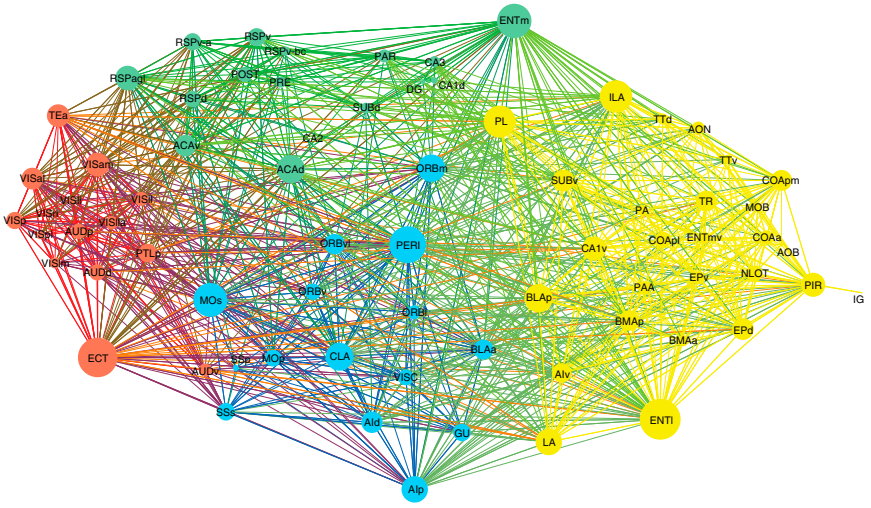


**Fig. 3.** Circuit diagram constructed using Gephi's weighted 3D force-directed algorithm. Node color indicates module number (M1, red; M2, blue; M3, green; M4, yellow), with size proportional to node degree (Fig. S1*C*). Edge color indicates output of correspondingly colored node; edge thickness is proportional to connection weight. "Very weak" and "weak" weights were dropped from analysis, minimizing the influence of false-positive results. Abbreviations are in Fig. S2.

found for 992 (18.9%) of all 5,256 ($73^2 - 73$) possible macroconnections. Assuming the curated literature representatively samples the 73-region matrix, the complete RCAM dataset would contain ~2,370 macroconnections (5,256 × 0.451), with a remarkably high average of 32 output association macroconnections per cortical region (2,370/73). However, RCAM number varied greatly for particular cortical regions (input range 9–51, output range 1–57). The dataset was derived from >16,000 RCAM connection reports, publicly available in the Brain Architecture Knowledge Management System (BAMS), expertly curated from >250 references in the primary literature.

**Network Analysis for Modules.** The RCAM dataset was first displayed in matrix format with column and row ordering following the cortical region sequence in the hierarchical structure–function nomenclature of Swanson-04 (16). Fig. 1 is a connection lookup table (matrix) automatically generated in BAMS2 Workspace (17) and provides a visual overview of connections that are reportedly present, are not present, or remain unexamined. Each of the 73 histologically defined cortical regions displays a unique set of input and output association connections with other cortical regions on the same side of the brain.

Modularity analyses (18) of the RCAM dataset that optimize a metric based on connection weights (Fig. S1 *A* and *B*) showed in connection matrix form (Fig. 2) that all 73 cortical regions cluster in one of four distinct modules (M1–M4) arranged in the matrix, such that more strongly connected modules are adjacent, and within-module regions more strongly connected are also adjacent (Fig. 2; Fig. S2 lists the 73 components with their abbreviations). This result was confirmed by using an alternate, circuit diagram graph analysis approach based on a force-directed algorithm (Fig. 3).

To distinguish visually whether module components are anatomically either interdigitated or segregated, they were mapped onto a topologically accurate cortical flatmap (16). Clearly, each module is a spatially continuous domain, with the four modules together covering the entire cortical mantle in a shell and core arrangement (Fig. 4*A*). This basic arrangement is also seen, although less clearly, in more familiar surface and cross-sectional views of the cortex (Fig. 5), and it is revealed in yet another view—all 1,923 association connections mapped onto the flatmap (Fig. 6).

Two modules form a complete shell (ring) around the medial edge of the cerebral cortex—roughly corresponding to the limbic region (lobe)—whereas the other two modules form a core within the shell—roughly corresponding to the cerebral hemisphere's lateral convexity. The caudal core (hemispheric) module (M1) contains visual and auditory areas and related association areas including posterior parietal and dorsal and ventral temporal. The rostral core (hemispheric) module (M2) contains somatic and visceral sensory–motor and gustatory areas and related association areas including orbital, agranular insular, and perirhinal. The dorsal shell (limbic) module (M3) contains the anterior cingulate and retrosplenial areas and major parts of the hippocampal formation, including medial entorhinal area, parasubiculum, presubiculum, postsubiculum, dorsal subiculum and dorsal field CA1, field CA3, and dentate gyrus. The ventral shell (limbic) module (M4) contains the most components, primarily regions belonging to the olfactory system, infralimbic and prelimbic areas (of the so-called medial prefrontal cortex), lateral amygdalar nucleus, and some hippocampal formation parts (lateral entorhinal area, ventral subiculum, and ventral field CA1).

**Small World, Hubs, and Rich Club.** Weighted network analysis of the RCAM dataset revealed two important hallmarks of local and global network organization—high clustering and high global efficiency, respectively. A high clustering value ($C = 0.084$), exceeding that found in a null model comprising a population of randomized networks ($C_{rand} = 0.057 \pm 6 \times 10^{-4}$, mean and SD for 10,000 randomized controls), indicates that if two cortical regions (nodes) are mutually connected, then it is highly probable (and more likely than expected by chance) that they also have common network neighbors. Such high clustering suggests that mutually connected regions have similar connectivity profiles as commonly found in local network clusters. The value of RCAM dataset's global efficiency ($G = 0.352$) is high and very close to those found in a population of randomized controls ($G_{rand} = 0.379 \pm 0.002$), indicating that the shortest paths between any two regions tend to comprise only a small number of steps, thus enabling effective global communication across the network. Together, high clustering and high efficiency (short path length) have been recognized as the defining features of small-world networks (19).

As in other connectome analyses, network measures allow us to identify nodes (here cortical regions) that are more strongly or

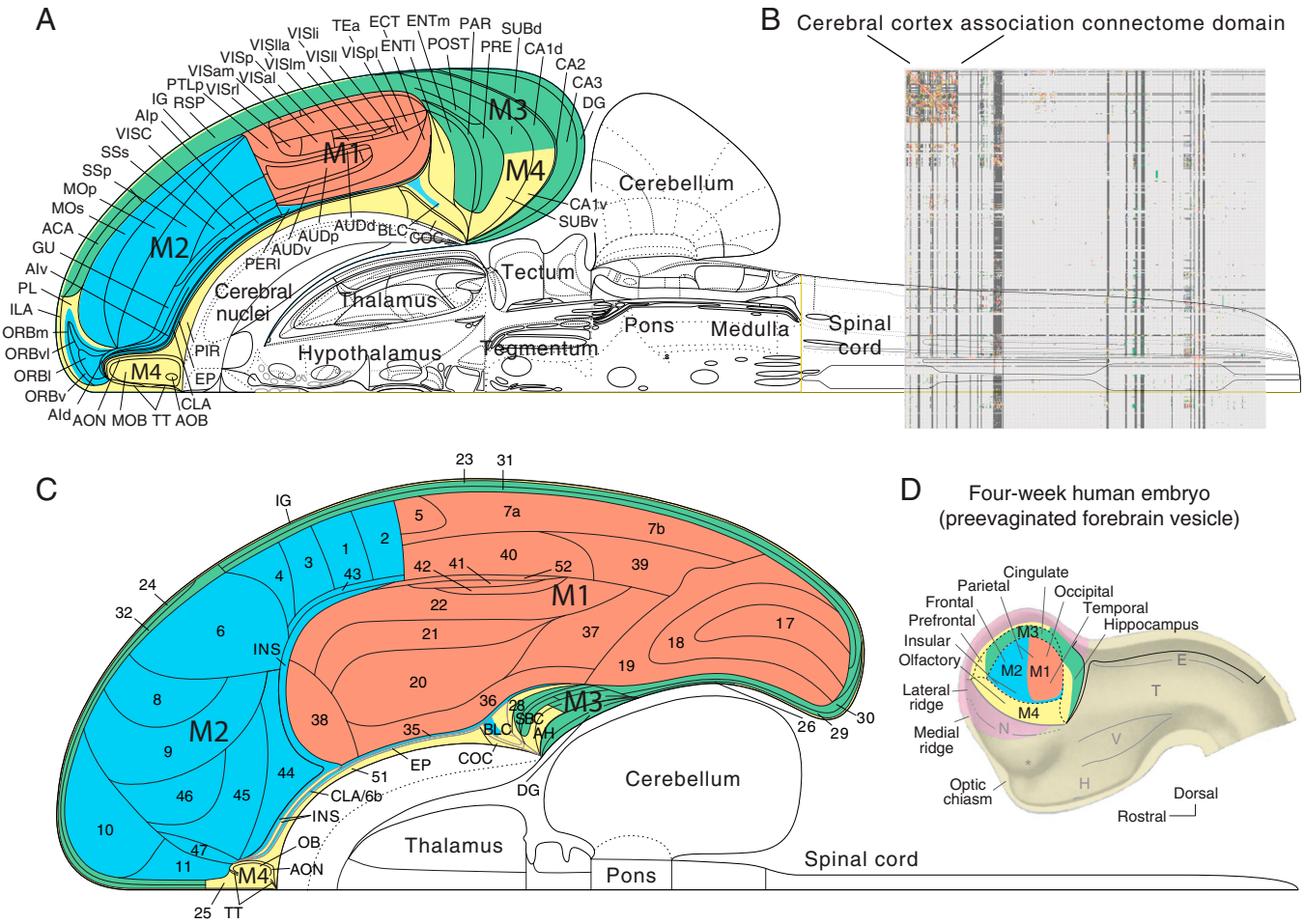


**Fig. 4.** Spatial distribution of cortical association modules. (*A*) Modules (M1–M4) in Figs. 2 and 3 plotted on a flatmap of right half of rat central nervous system (16); M1, red; M2, blue, M3, green, M4, yellow. See ref. 16 for high-resolution details. (*B*) The cortical association connectome (Fig. 1) shown in the context of the complete rat central nervous system connectome that has just 15% matrix coverage (fill ratio) because most literature outside the cortical association domain is not yet expertly curated (44). Abbreviations are in Fig. S2. (*C*) Histologically defined human cortical regions corresponding to rat cortical regions (correspondence documented in Fig. S2) plotted on a flatmap (45) and color coded as in *A*. AH, Ammon's horn; AON, anterior olfactory nucleus; BLC, basolateral amygdalar complex; CLA/6B, claustrum/layer 6b; COC, cortical amygdalar complex; DG, dentate gyrus; EP, entopeduncular nucleus; INS, insular region; OB, olfactory bulb; TT, tenia tecta; SBC, subicular complex. Numbers correspond to Brodmann's areas (Fig. S2). (*D*) Predicted fate map of major cerebral cortical regions with general location of rat M1–M4 (color coded as in *A* and *C*); illustrated on the right embryonic forebrain vesicle viewed from medial aspect (4-wk human; equivalent to 11-d rat, 9/10-d mouse); adapted from ref. 46. E, epithalamus; H, hypothalamus; N, cerebral nuclei; T, dorsal thalamus; V, ventral thalamus.

more centrally connected within the network, corresponding to so-called network hubs (20, 21). We identified the hubs in the cortical association network by computing four centrality measures (Fig. S1*C*) and ranking nodes according to their aggregate centrality score (Fig. S2, red cortical regions). The set with the highest scores (a value of 4, indicating high rankings across all four measures) comprised three nodes: ectorhinal, perirhinal, and lateral entorhinal areas. Interestingly, these three hubs form a topographically continuous patch of cortex that is also highly mutually connected (see discussion of rich club below). In humans, this patch generally shows the earliest, most severe pathological changes in Alzheimer's disease (22) and is implicated in temporal lobe epilepsy (23).

Another significant aspect of network organization is the presence of a "rich club," defined as a set of highly connected nodes (regions) that are also densely connected with each other (24, 25). Rich-club analysis (Fig. S3 *A* and *B*) revealed three innermost-circle rich-club nodes (lateral entorhinal area, medial entorhinal area, and claustrum) positioned within a set of 15 rich-club nodes with the greatest statistical significance (adjusted $P = 1.02 \times 10^{-11}$; false discovery rate set to 0.001). These 15 nodes are distributed within all four modules, with the greatest participation in the ventral limbic module, M4. Anatomical analysis by inspection of the reference atlas (16) readily shows that all but one (field CA1v) of these rich-club nodes form a topographically continuous U-shaped band that can be divided into a caudodorsal cortical plate pole (P1), a rostrodorsal cortical plate pole (P2), and between them a ventral cortical subplate pole (P3). The three highest-ranked hubs form a patch in P3 (Fig. S3*C*), and the lateral entorhinal area is the only cortical region that is both one of these three hubs and one of the three innermost circles of rich-club nodes. The lateral entorhinal area forms the richest set of association connections of any cerebral cortical region in rat (26).

**Connection Patterns.** Analysis of global major connection weight patterns between all network nodes yielded statistically significant asymmetries (Fig. S1 *D* and *E*) indicating overrepresentation and underrepresentation of weight class combinations in bidirectional connections between region pairs ($P < 0.0014$) and

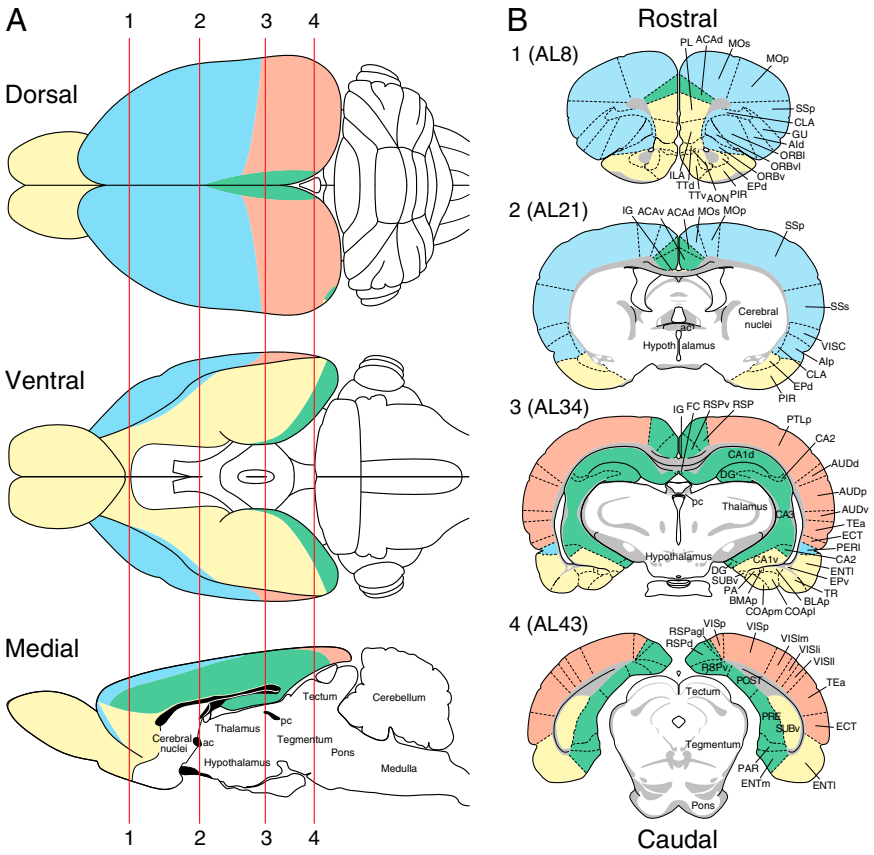


**Fig. 5.** Module distribution on surface and transverse views. (*A*) Surface views of the rat brain with four RCAM module domains color coded as in Figs. 3 and 4. Four vertical red lines indicate transverse levels through the brain shown in *B*. (*B*) Four transverse levels through the rat brain with modules color coded as in *A*; specifically, Atlas levels (AL) 8, 21, 34, and 43 of ref. 16 are shown. ac, anterior commissure; pc, posterior commissure; all other abbreviations are in Fig. S2.

showing that highly asymmetric weight combinations between two such nodes are less frequently encountered in the empirical connection matrix than expected if weights are randomly assigned to existing connections. This result implies at least partly "hard-wired," genetically determined biases in information flow through the cortical association macroconnectome network.

The implications of these results for connection patterns within and between modules were then assessed because all but

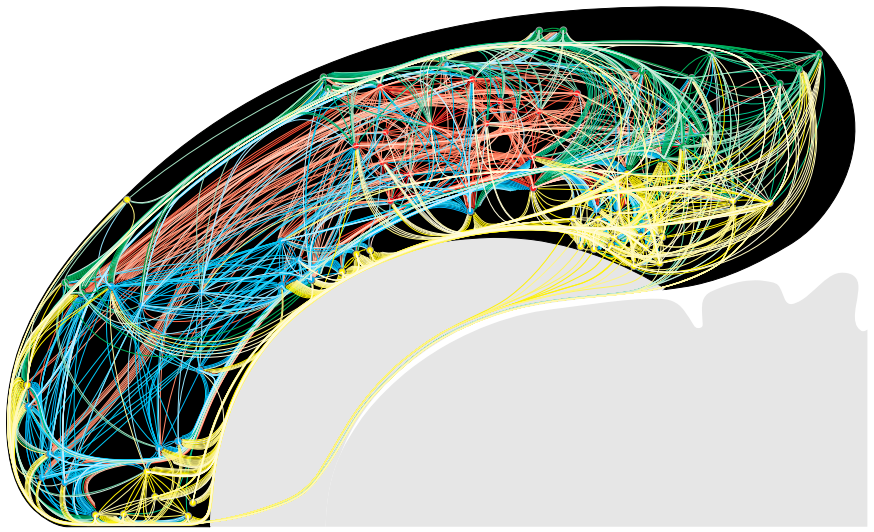

**Fig. 6.** All 1,923 RCAMs mapped onto the flatmap and color coded as in Figs. 3 and 4. Connection routes were placed to follow known white-matter tracts (16) and/or to follow the shortest path between origin and termination nodes (circles), without crossing unrelated nodes between them, for clarity. For a high-resolution view with labeled nodes, see Fig. S4.

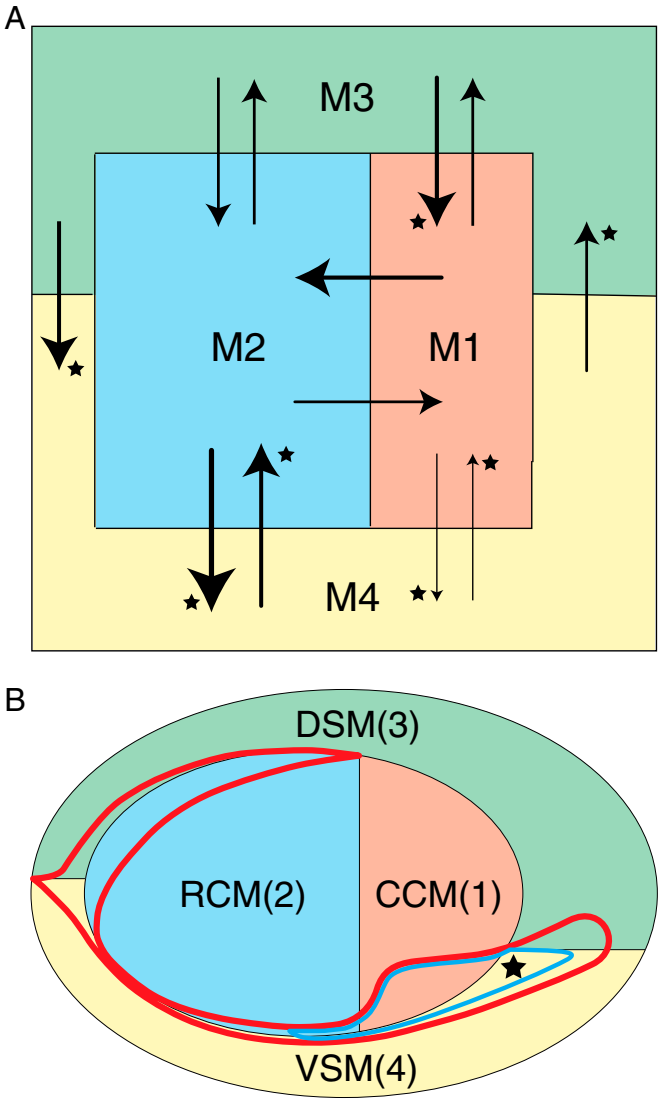


**Fig. 7.** Basic logic of cortical association module organization. (*A*) Schematic diagram of topological relationships between cortical association modules M1–M4 (color-coded as in Figs. 4 and 5 and abstracted from the patterns in Fig. 4 and Fig. S3) with aggregate connection weights between them. Weight estimates are based on total connection number, scaled from 1 to 5 (indicated by line thickness); statistically significant differences (Table S3) are starred. (*B*) An alternate schematic view of topological relationship between modules M1–M4, rich-club regions (within thick red outline), and three highest ranked hubs (within thinner blue line with star, which indicates the most connected node of all, the lateral entorhinal area) nested in rich-club territory. The rich club and hubs are shown on the flatmap in Fig. S3C. CCM, caudal core module (M1, red); DSM, dorsal shell module (M3, green); RCM, rostral core module (M2, blue); VSM, ventral shell module (M4, yellow).

two cortical regions (anterior olfactory nucleus and indusium griseum in M4) also connect with other modules (Fig. 2). Connection weight distribution analysis within and across modules M1–M4 revealed 894 intermodular association connections, together establishing bidirectional connections between each of the four modules (Fig. 7*A* and Tables S1 and S2). Overall, ranked qualitative estimates of connection weight indicate asymmetries in intermodular bidirectional communication, again implying at least partly hardwired biases in information flow through the RCAM network, at the level of modules.

As expected (Fig. 2), intramodular connections tend to be strong, whereas intermodular connections tend to be moderate at best (Tables S1 and S2). Furthermore, the distribution of major unidirectional (Fig. 7*A* and Tables S1–S3) connections within and between modules also indicates that each module has a unique, statistically significant pattern of association connections.

Sets of cortical association outputs and inputs between the three rich-club poles differ, and asymmetries are related to connection weight categories (Tables S4 and S5). Two organization features are obvious: major connections between the three poles are asymmetric and all share the same orientation, whereas medium-weight connections all share the opposite orientation; and between sets of poles only two of the three connection weights share the same orientation. Clearly, information flow is heavily biased at this third level of analysis, in the network formed between the three rich-club poles.

**Module Configuration and Data Coverage.** A critical question in statistical network analysis based on empirical data is: What minimum matrix coverage ("fill ratio") is required for stable overall patterns to emerge? This question was examined in two ways for our data. First, during curation, nine sequential versions were saved of the RCAM matrix, with coverage from 22% to 81%. Visual inspection showed that module number and composition depended on coverage, with a stable pattern emerging after 65% coverage was achieved (Fig. 8*A*). Second, module configuration stability as a function of matrix coverage was tested by performing random deletion of connectional data (Fig. 8 *B* and *C*). The median number of modules (100 random deletions) approached four and then stabilized at ∼60% coverage, confirming a minimum coverage of approximately two-thirds for qualitatively stable patterns. In our dataset, final coverage for all intermodular and intramodular connection subsets ranged from 72% to 93% (Table S6).

**Bridge to Human Cortical Connectome.** A highly desirable goal is to leverage detailed systems neuroscience data from animals to better understand mechanisms generating cognition in humans, where currently experimental circuit analysis faces major obstacles. For example, experimental animal histological analysis of circuitry operates at the nanometer to micrometer level for subcellular and cellular resolution, whereas human imaging methods operate at the millimeter level for gross anatomical resolution. To stimulate interactions between basic animal research and translational human connectome research, the anatomical distribution of association macroconnection modules, hubs, and rich-club members in rat were mapped onto proposed equivalents in human cortex (Fig. 4*C* and Fig. S3*D*), based on the preponderance of current evidence about the relationship between cortical parcellation in rat and human (Fig. S2).

The underlying rationale for this approach goes back to Brodmann (27), who examined >60 species representing seven orders and hypothesized that there is a basic mammalian plan of cortical structural regionalization that, like the overall body plan, is differentiated in different species. This generalization has been broadly confirmed, so it is reasonable to hypothesize that synaptic connectional data gathered in nonhuman mammals—like rodents (Figs. 1 and 2) and monkeys (28)—can be used to help interpret and propose testable hypotheses about cerebral cortical biological mechanisms in humans (at least at the macroconnection level), where almost no such data exists or is even possible with current MRI technology as discussed above.

## Discussion

Our results provide an alternative to the traditional approach of describing the most general level of cerebral cortex organization—even in rodents—with reference to "lobes" named arbitrarily for overlying bones and to linear streams of connections identified by selective functional analysis. Systematic, data-driven, network analysis of the rat cortical association connectome instead reveals

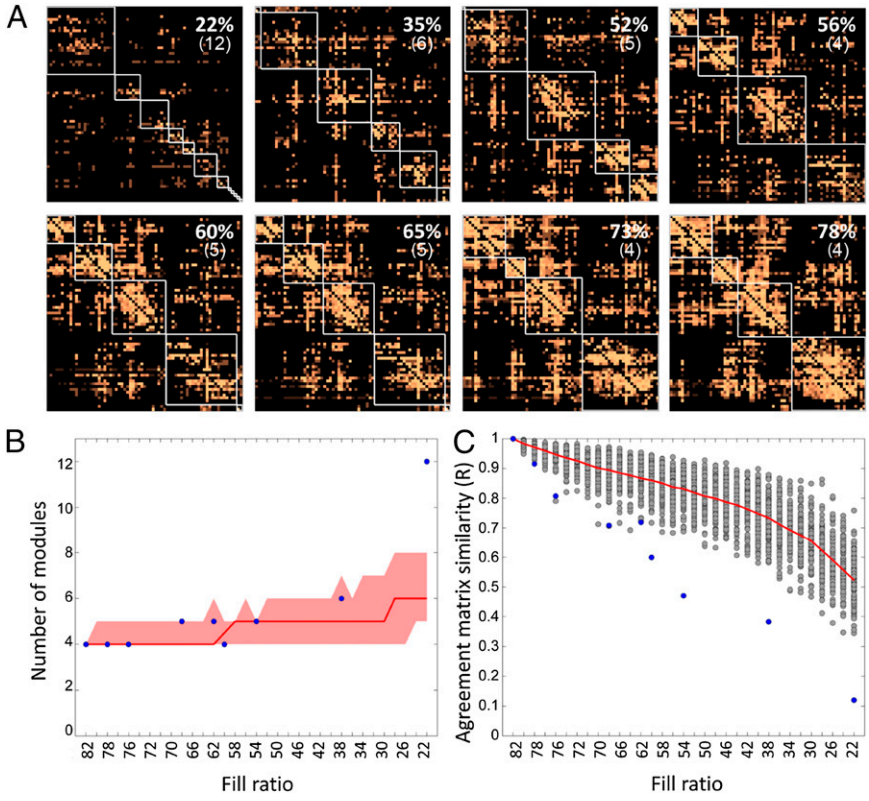


**Fig. 8.** Data coverage effect on final connectome pattern. (*A*) Eight versions of cortical association connectome saved during curation with indicated percent coverage (fill ratio) and number of modules (in parentheses). Matrices are based on 69 regions because the total increased to 73 during the process of curation. (*B*) Empirical matrix module number (blue point at 81% coverage), eight less-covered matrices (remaining eight blue points), median module number for randomly degraded matrices (solid red line) with corresponding minimum (red shaded area lower bound) and maximum (red shaded area upper bound). (*C*) Agreement matrix similarities between empirical matrix (81% coverage) and eight incompletely covered matrices (blue points) and randomly degraded matrices (gray points), expressed as Pearson correlation of upper matrix triangles.

novel design features (Fig. 7*B*). Based on its association connections, the entire rat cerebral cortex (*i*) is divided into four topographically and topologically nonoverlapping modules with a core–shell organization, (*ii*) has a topographically continuous rich club of regions/nodes with three poles that together span restricted parts of all four modules, and (*iii*) has its three highest ranked hubs clustered together within the caudal rich-club pole. Furthermore, each of the 73 cortical regions has a unique set of input and output association connections, and each of the four modules has a unique pattern of intramodular and intermodular connections—a unique connectional identity that overall tends to minimize connection lengths. Finally, each rich-club pole has a unique pattern of asymmetrical input and output connections with the other two poles.

The four association connection modules may thus form basic morphological units of the rat cerebral cortex. This possibility is strengthened by their predicted general localization in the earliest recognizable stage of cortical embryonic development (Fig. 4*D*). Molecular genetic mechanisms generating this regionalization and wiring pattern remain to be clarified.

The analysis strategy developed here provides a framework for going on to determine the complete cortical mesoconnectome (at the neuron-type level) and then microconnectome (at the individual neuron level) in rodents and to establish in various species the general plan of mammalian cortical organization and its differentiable features, which would include commissural connections as well as extrinsic inputs and outputs.

More globally, the structural microconnectome of nematode worms began more than a century ago (29) with light microscopy and is the only generally completed effort thus far (30). More limited analyses in mammals have usually focused on isocortical regions of the cortical plate rather than the entire cortical mantle as here. Metaanalyses revealed four structure–function modules (visual, auditory, somatomotor, fronto-limbic) in cat (31, 32) and five modules quite different from those identified here in macaque, although some striking similarities in hub and rich-club members were identified (33). Discrepancies with results presented here may be due to a combination of factors, including differences in species, nomenclature, connection weight scaling, statistical methods, and dataset completeness. Results from two recent mouse studies (34, 35) differed from those presented here, primarily due to less robust connection weight scaling, different network analysis methods, and much lower degree of matrix coverage (Table S7 and Fig. 8).

Our results encourage completion of the rodent central nervous system connectome at the same level of data accuracy and reliability, and of network analysis, displayed for the cerebral cortex (Fig. 2). The current level of curation in our knowledge management system is shown in Fig. 4*B*, suggesting a systematic curation strategy for the 10 basic topographic divisions of the central nervous system (36, 37), starting most productively with the cerebral cortex (38) and then progressing caudally through the cerebral nuclei, thalamus, hypothalamus, tectum, tegmentum, pons, cerebellum, medulla, and spinal cord (Figs. 4*A* and 5*A*, medial). A complete rat connectome involves a matrix of 503 gray matter regions with 252,506 elements (macroconnections) on each side of the central nervous system (16). Even this comprehensive matrix of macroconnections would be incomplete. At the macroscale, a complete structure–function neurome would also include peripheral ganglia and the muscles, glands, and other

body parts innervated. As microscale connectome maps continue to expand (39), a final point of convergence may be a nested multiscale "zoomable" map (12, 13) of a mammalian nervous system that reveals nonrandom network attributes of local neural circuitry as well as large-scale nervous system structure–function subsystems.

The global cortical association connectome presented here is for the presumably "normal" adult albino rat, and similar data are being generated for adult mouse (34, 35). It is now technically possible to construct similar connectomes in rodent models of disease where cortical connectopathies (39) are hypothesized, and it will be important to develop effective statistical methods for testing these hypotheses by comparing connectomes at the cellular (micrometer) and synaptic (nanometer) levels for a particular species—an approach already being applied successfully at the regional (millimeter) level for human imaging studies (40). It will be even more challenging to develop rigorous comparisons of connectomes between species, where the difficult problem of establishing homologies like those proposed here between rodent and human cortical regionalization (Fig. S2) is fundamental (41). However, developments along these lines could eventually lead to connectome-scale association studies at multiple scales of resolution and even involving multiple species—similar in principle to genome-scale association studies (42) and perhaps even correlated with them as a powerful new approach to the classification, etiology, and treatment of connectopathies underlying mental health disease.

## Materials and Methods

Methods for the underlying analysis are described in detail in *SI Materials and Methods*. Briefly, data were curated for the entire cerebral cortical mantle, including both isocortex (neocortex) and allocortex (paleocortex and archicortex), and thus including all regions associated with the cortical plate and underlying cortical subplate (16). All relevant data in the primary literature were interpreted in the only available standard, hierarchically organized, annotated nomenclature for the rat (16) and compiled with supporting metadata in BAMS (brancusi.usc.edu; refs. 8, 43, and 44) by using descriptive nomenclature defined in the Foundational Model of Connectivity (12, 13). Cortical association connection reports in BAMS were encoded with ranked qualitative connection weights based on pathway tracing methodology, injection site location and extent, and anatomical density. Network analysis for modularity, small world organization, hubs, and rich club followed standard procedures described in refs. 18 and 19.


1. Kandel ER, Hudspeth AJ (2013) The brain and behavior. *Principles of Neural Science*, eds Kandel ER, Schwartz JH, Jessell TM, Siegelbaum SA, Hudspeth AJ (McGraw-Hill, New York), 5th Ed, pp 5–20.
2. Swanson LW (2012) *Brain Architecture: Understanding the Basic Plan* (Oxford Univ Press, Oxford), 2nd Ed.
3. Catani M, Mesulam M (2008) What is a disconnection syndrome? *Cortex* 44(8): 911–913.
4. Nieuwenhuys R, Voogd J, van Huijzen C (2008) *The Human Central Nervous System* (Springer, Berlin), 4th Ed.
5. Bota M, Dong H-W, Swanson LW (2003) From gene networks to brain networks. *Nat Neurosci* 6(8):795–799.
6. Sporns O, Tononi G, Kötter R (2005) The human connectome: A structural description of the human brain. *PLOS Comput Biol* 1(4):e42.
7. Bohland JW, et al. (2009) A proposal for a coordinated effort for the determination of brainwide neuroanatomical connectivity in model organisms at a mesoscopic scale. *PLOS Comput Biol* 5(3):e1000334.
8. Bota M, Dong H-W, Swanson LW (2005) Brain architecture management system. *Neuroinformatics* 3(1):15–48.
9. von Economo C (1926) Ein koeffizient für die organisationshöhle der grosshirnrinde. *Klin Wochenschr* 5:593–595.
10. Karlsen AS, Pakkenberg B (2011) Total numbers of neurons and glial cells in cortex and basal ganglia of aged brains with Down syndrome—a stereological study. *Cereb Cortex* 21(11):2519–2524.
11. Ribeiro PF, et al. (2013) The human cerebral cortex is neither one nor many: Neuronal distribution reveals two quantitatively different zones in the gray matter, three in the white matter, and explains local variations in cortical folding. *Front Neuroanat* 7:28.
12. Swanson LW, Bota M (2010) Foundational model of structural connectivity in the nervous system with a schema for wiring diagrams, connectome, and basic plan architecture. *Proc Natl Acad Sci USA* 107(48):20610–20617.
13. Brown RA, Swanson LW (2013) Neural systems language: A formal modeling language for the systematic description, unambiguous communication, and automated digital curation of neural connectivity. *J Comp Neurol* 521(13):2889–2906.
14. Bota M, Swanson LW (2007) The neuron classification problem. *Brain Res Brain Res Rev* 56(1):79–88.
15. Meynert T (1867–1868) Der bau der Gross-Hirnrinde und seine örtlichen verschiedenheiten, nebst einem pathologisch-anatomischen corollarium. *Vierteljarsschr Psychiat* 1:77–93. 198–217 (1867), 2:88–113 (1868).
16. Swanson LW (2004) *Brain Maps: Structure of the Rat Brain. A Laboratory Guide with Printed and Electronic Templates for Data, Models and Schematics* (Elsevier, Amsterdam), 3rd Ed.
17. Bota M, Talpalaru S, Hintiryan H, Dong H-W, Swanson LW (2014) BAMS2 workspace: A comprehensive and versatile neuroinformatic platform for collating and processing neuroanatomical connections. *J Comp Neurol* 522(14):3160–3176.
18. Rubinov M, Sporns O (2010) Complex network measures of brain connectivity: Uses and interpretations. *Neuroimage* 52(3):1059–1069.
19. Watts DJ, Strogatz SH (1998) Collective dynamics of 'small-world' networks. *Nature* 393(6684):440–442.
20. Sporns O, Honey CJ, Kötter R (2007) Identification and classification of hubs in brain networks. *PLoS ONE* 2(10):e1049.
21. van den Heuvel MP, Sporns O (2013) Network hubs in the human brain. *Trends Cogn Sci* 17(12):683–696.
22. Braak H, Rüb U, Schultz C, Del Tredici K (2006) Vulnerability of cortical neurons to Alzheimer's and Parkinson's diseases. *J Alzheimers Dis* 9(3, Suppl):35–44.
23. de Curtis M, Paré D (2004) The rhinal cortices: A wall of inhibition between the neocortex and the hippocampus. *Prog Neurobiol* 74(2):101–110.
24. Colizza V, Flammini A, Serrano MA, Vespignani A (2006) Detecting rich-club ordering in complex networks. *Nat Phys* 2:110–115.
25. van den Heuvel MP, Sporns O (2011) Rich-club organization of the human connectome. *J Neurosci* 31(44):15775–15786.
26. Swanson LW, Köhler C (1986) Anatomical evidence for direct projections from the entorhinal area to the entire cortical mantle in the rat. *J Neurosci* 6(10):3010–3023.
27. Brodmann K (2006) *Brodmann's Localization in the Cerebral Cortex: The Principles of Comparative Localisation in the Cerebral Cortex Based on the Cytoarchitectonics*; trans Garey L (Springer, New York).
28. Bakker R, Wachtler T, Diesmann M (2012) CoCoMac 2.0 and the future of tract-tracing databases. *Front Neuroinform* 6:30.
29. Goldschmidt R (1909) Das nervensystem von *Ascaris lumbricoides* und *megalocephala*. III. *Z Wiss Zool* 92:306–357.
30. Jarrell TA, et al. (2012) The connectome of a decision-making neural network. *Science* 337(6093):437–444.
31. Scannell JW, Blakemore C, Young MP (1995) Analysis of connectivity in the cat cerebral cortex. *J Neurosci* 15(2):1463–1483.
32. de Reus MA, van den Heuvel MP (2013) Rich club organization and intermodule communication in the cat connectome. *J Neurosci* 33(32):12929–12939.
33. Harriger L, van den Heuvel MP, Sporns O (2012) Rich club organization of macaque cerebral cortex and its role in network communication. *PLoS ONE* 7(9):e46497.
34. Zingg B, et al. (2014) Neural networks of the mouse neocortex. *Cell* 156(5):1096–1111.
35. Oh SW, et al. (2014) A mesoscale connectome of the mouse brain. *Nature* 508(7495): 207–214.
36. Nauta WJH, Feirtag M (1986) *Fundamental Neuroanatomy* (Freeman, New York).
37. Swanson LW (2000) What is the brain? *Trends Neurosci* 23(11):519–527.
38. Swanson LW (2005) Anatomy of the soul as reflected in the cerebral hemispheres: Neural circuits underlying voluntary control of basic motivated behaviors. *J Comp Neurol* 493(1):122–131.
39. Lichtman JW, Sanes JR (2008) Ome sweet ome: What can the genome tell us about the connectome? *Curr Opin Neurobiol* 18(3):346–353.
40. Zalesky A, Cocchi L, Fornito A, Murray MM, Bullmore E (2012) Connectivity differences in brain networks. *Neuroimage* 60(2):1055–1062.
41. Bota M, Arbib MA (2004) Integrating databases and expert systems for the analysis of brain structures: Connections, similarities, and homologies. *Neuroinformatics* 2(1): 19–58.
42. McCarroll SA, Feng G, Hyman SE (2014) Genome-scale neurogenetics: Methodology and meaning. *Nat Neurosci* 17(6):756–763.
43. Bota M, Swanson LW (2010) Collating and curating neuroanatomical nomenclatures: Principles and use of the Brain Architecture Knowledge Management System (BAMS). *Front Neuroinform* 4:3.
44. Bota M, Dong H-W, Swanson LW (2012) Combining collation and annotation efforts toward completion of the rat and mouse connectomes in BAMS. *Front Neuroinform* 6:2.
45. Swanson LW (1995) Mapping the human brain: past, present, and future. *Trends Neurosci* 18(11):471–474.
46. Swanson LW (2000) Cerebral hemisphere regulation of motivated behavior. *Brain Res* 886(1–2):113–164.

# Supporting Information

## Bota et al. 10.1073/pnas.1504394112

### SI Materials and Methods

**Cortical Histological Parcellation Granularity.** All connection-related data were mapped onto the Swanson-04 hierarchical nomenclature for the rat central nervous system (1). In this classification scheme, gray-matter regions are regarded as comparable to species in animal taxonomy, and gray-matter subregions are comparable to subspecies (2). All but 2 of the 80 cortical entities in the RCAM matrix are at the level of cortical gray-matter regions thus defined. One exception is the anterior olfactory nucleus, which has five parts, each considered a gray matter region in the nomenclature hierarchy. For present purposes, the anterior olfactory nucleus (superstructure parent) is considered a single entity in the matrix because there is a lack of accurate and reliable connectional data for the five parts (children) and because recognition of various parts varies considerably in the literature (1). The other exception is field CA1 of Ammon's horn, where two subregions, dorsal and ventral, were recently recognized (3), just as dorsal and ventral gray matter regions in the adjacent subiculum have long been recognized (1). Finally, four tiny regions—the fasciola cinerea, posteromedial visual area, and posterior auditory area of the cortical plate, and sublayer 6b (sometimes called layer 7) of the cortical subplate—have not been included in the analysis because accurate and reliable association connectional data were not available for them.

**Annotation and Collation Methodology for Connection Report Weights.** Our methodology for annotating and collating rat connectional data from the primary neuroanatomical research literature has been presented (4, 5). Overall, the general procedure involved four sequential steps: first, eliminate connection reports based on older (nonexperimental and degeneration) methodology and interregional injection sites; second, choose connection reports based on the best method and injection site(s); third, choose connection report with the greatest anatomical density; and fourth, use the latter for the region of interest connection matrix cell and then for network analysis.

Here we concentrate on procedures followed specifically to create the RCAM reports used for statistical network analysis (see below). The starting point was ∼72,000 connection reports for the central nervous system that are (*i*) annotated and collated from the primary neuroanatomical literature and recorded in BAMS (brancusi.usc.edu), and (*ii*) based on experimental pathway tracers transported anterogradely, retrogradely, or in both directions within axons. Reports based on experimental degeneration (lesion) and normal (no experimental lesions or tracer injections) methods, which have considerably less validity (6), were eliminated from consideration.

From this, a subset of reports related only to RCAMs was extracted, and this subset was further pruned by eliminating connection reports with interregional tracer injection sites—that is, injection sites extending significantly from the gray-matter region of interest into one or more additional cortical gray matter regions. These reports were eliminated because they are ambiguous: reported pathways could be associated with any gray matter region significantly labeled by the injection site, without independent verification from other experiments. This pruning yielded >16,000 connection reports from >250 references in the primary literature.

**Ranking Weights for the Connection Matrix.** The next procedure involved choosing one weight for a connection between two regions of interest when multiple reports for that connection exist in BAMS. In our matrix of 73 cortical regions, there are 5,256 ($73^2 - 73$) possible macroconnections, and we started with >16,000 connection reports. The key consideration is that a connection report contains data about one anatomical pathway labeled in a particular experiment; typically, the pathway is a subset of the global synaptic connection established from one gray-matter region to another gray-matter region (7). This consideration is critically important because extensive evidence demonstrates that cortical gray-matter regions are not, as a rule, structurally homogeneous. Thus, in general, single experimental tracer injections presumably label only part of the global connection pattern between two gray-matter regions, with the part (pathway) depending on the extent and location of injection site.

Strictly, in the present context, connection reports may contain information about pathways (macropathways) and/or connections (macroconnections), but almost always the former; a macroconnection is the entire directed connection pattern established from one gray-matter region (the origin) to another gray-matter region (the termination). For network analysis, a macroconnection is an element (cell) in a matrix or a directed edge between two nodes in a graph. Typically, there are multiple connection reports (each reporting a pathway) for a macroconnection of interest; the following ranking procedure was designed to choose from the available literature the most accurate and reliable macroconnection weight for each cell in the connection matrix used for network analysis.

For choosing one weight per macroconnection of interest, relevant connection reports were ranked on three criteria: the most accurate and reliable tracer methodology, optimal tracer injection site(s) relative to the region of interest, and highest anatomical density of relevant pathway tracer labeling (the highest connection weight).

The first consideration was pathway tracer methodology used for data acquisition. The set of >16,000 RCAM reports was therefore organized in three subsets (5) based on this criterion. For methods used in this dataset, the most accurate and reliable subset (highest validity) of connection weights includes at the top (*i*) injections of the anterograde pathway tracer *Phaseolus vulgaris* leucoagglutinin (PHAL) confined within the borders of regions of interest, and (*ii*) such connections confirmed with retrograde tracers. If retrograde tracer data were not available, then connection reports based just on PHAL experiments were used.

The second subset includes at the top connections reported with biocytin or cholera toxin subunit B as anterograde tracers, confirmed with retrograde tracers. If confirmatory retrograde tracing was unavailable, then anterograde tracer data alone was used. If no anterograde tracer data were available for a connection of interest, then retrograde tracer data alone was used if based on tracers minimally labeling axons-of-passage. At the lower end of the spectrum, the third, least accurate and reliable subset (lowest validity) of connection weights includes connection reports where no information was published about injection site distribution (whether large or small) and from analyses based simply on injections of the anterograde tracer, tritiated amino acids (autoradiographic method), or the anterograde/retrograde tracer, HRP (HRP method; alone or with wheat germ agglutinin).

The resulting set of connection reports collated in BAMS and ranked on the basis of methodology was then reranked, if necessary, on the basis of the second criterion—injection site location and extent within the region of interest. Two categories were created for ranking multiple connection reports for a region of interest based on this critically important factor. As discussed

above, reports with an injection site extending significantly into another region or regions (an interregional injection site) were eliminated from consideration at the start; only intraregional injection sites were considered.

Category 1 (of intraregional injection sites) includes connection reports associated with experiments involving large tracer injections extending throughout, or involving a large part of, the region of interest—labeling all subregions with no spread outside the borders of the region as a whole. If no such experiments were registered in BAMS, then connection reports associated with large injection sites displaying slight spread outside the region of interest were chosen. The set of connections labeled by all category-1 injection sites for a region of interest were entered into BAMS because, as noted above, regions of interest generally are not homogeneous.

If no category-1 reports were found in BAMS, category-2 reports were sought. They deal with cortical plate regions (cortical subplate regions are not layered) and include combinations of experiments, with an individual experiment (injection site) labeling a subset of layers and the combination of injection sites (experiments) labeling as many layers (and their physical extent) as possible in the region of interest. For these combined injection sites, the highest weights of combined sets of terminations (targets) or origins (sources) were used.

If information about the spread of an injection site relative to a region of interest was unclear from collated reports in BAMS, the information was reannotated and recollated as well as possible from information provided in the relevant reference and to the best of the collator's expert knowledge and interpretation. To double-check accuracy, in this step we also reannotated connection reports associated with very large injection sites that extended through two or more of the 73 cortical regions included in this analysis.

The third ranking criterion is anatomical density. Depending on tracer, relevant data included retrogradely labeled neuron cell bodies for pathway origin (from/source) and anterogradely labeled axon terminals for pathway termination (to/target), leaving out of consideration axons themselves, which simply form the route (in tracts) between origin and termination (7). Axon terminal (bouton) is a traditional light-microscopic term that indicates the presence of a synapse when confirmed electron-microscopically (7). As described below, each connection report has an associated ranked qualitative weight with 1 of 11 values in BAMS (4–7).

During the manual verification of the most accurate and reliable connection weights used to construct the RCAM matrix, reports in BAMS with the value "exists" were also reannotated and recollated, reducing their number to just 11 (of 1,923). In addition, connection reports involving field CA1 were manually reannotated and recollated in terms of ventral and dorsal subregions (3).

Connection reports with the value "not present" were added to the dataset only if this conclusion was stated in the text of associated references or if complete sets of Atlas Levels, photographic plates, or drawings were included for relevant regions of the cerebral cortex and no terminal fields were displayed.

In summary, for a given cell in the connection matrix, the connection weight chosen when multiple connection reports are available in BAMS was associated with the highest ranked method and most complete intraregional injection site (or combination of intraregional injection sites). When only incomplete injection sites were available for the highest ranked method, connection reports for lower-ranked methods with more complete injection sites were compared and considered.

As a first step of network analysis, the subset of highest ranked connection reports for each region of interest was manually inserted into the BAMS2 Workspace (5) and an initial RCAM matrix was automatically produced (Fig. 1). The expert manual curation of >16,000 connection reports took >4,000 h. The connectional data are available online at BAMS (brancusi1.usc.edu/connections/grid/168).

**Connection Weight Scaling Methodology for Network Analysis.** Various sets of central nervous system parts in other mammals subjected to statistical network analysis used only binary values indicating the presence or absence of connections (8–10). In contrast, we begin by encoding ranked qualitative connection weights from the literature using 11 categories. From 1 to 11, they are: very strong, strong, moderate/strong, moderate, weak/moderate, weak, very weak, axons-of-passage, not present, unknown (no data), and exists (weight unknown). For purposes of our network analysis, axons-of-passage are equivalent to very weak, and exists is equivalent to moderate. For the use of this ranking scheme in BAMS, see ref. 4; for practical application in a specific neurohistological analysis, see ref. 11. When network analysis was applied to the dataset, the "unknown" (no data) category was considered "not present." Thus, the set of ranked qualitative values used for network analysis included 8 values.

Next, these ranked qualitative connection weights were transformed to approximately logarithmically spaced weights for network analysis. The primary research literature dealing with experimental pathway tracing experiments in rat and macaque suggests that the most realistic scale for ranked qualitative values is exponential rather than linear. A $10^5$ exponential scale was adopted for such results in macaque cerebral cortex (12), and a similar approach was found to be most appropriate here, although a $10^4$ exponential scale fit the rat data better (for example, see refs. 13–16).

Specifically, connection weights were transformed from eight distinct values of ranked qualitative connection weights (not present, very weak, weak/moderate, moderate, moderate/strong, strong, and very strong) to approximately logarithmically spaced weights, with weights spanning approximately four orders of magnitude (Fig. S1*A*). These 8 (of the original 11) values were considered for these purposes to form an ordinal scale. Visual inspection of tracing data suggested a more linear spacing of connection weight categories at the high end of the scale—for example, between strong and very strong connections. This observation was incorporated into the scaling model of connection weights, which was more logarithmic for weak weights and more linear for strong weights.

Overall, the largest number of RCAMs was classified as moderate, with fewer connections at the extreme ends of the scale, very weak and very strong (Fig. S1*B*).

**Network Analysis Methods.** Network analyses were carried out on the directed and log-weighted RCAM matrix (Figs. 1 and 2) by using tools collected in the Brain Connectivity Toolbox (www.brain-connectivity-toolbox.net). Detailed descriptions of network measures can be found in ref. 17. Rat cortical gray-matter regions are referred to as nodes of the RCAM network.

Modularity analysis was carried out as follows. The Louvain algorithm (18) for detecting modules by maximizing a modularity metric (18, 19) adapted for use with weighted networks was run 10,000 times. The single module partition for which the modularity metric became maximal ($Q_{max} = 0.3576$) was selected and formed the basis for all further analyses of network modules.

Computing global network measures on the weighted connection matrix (20) revealed a number of characteristic attributes such as high clustering (clustering coefficient $C = 0.084$; $C_{rand} = 0.057 \pm 6 \times 10^{-4}$, mean and SD for 10,000 randomly rewired networks) and high global efficiency ($G = 0.352$; $G_{rand} = 0.379 \pm 0.002$). Rewiring of the networks comprising the random null model was carried out following a commonly used procedure equivalent to a Markov switching algorithm (21), preserving the number of incoming and outgoing connections on all nodes.

High clustering and high global efficiency are generally considered possible indicators of small world organization in networks such as those considered here.

Network hubs were determined on the basis of four distinct nodal centrality measures: node degree, node strength, node betweenness centrality, and node closeness centrality. Degree is defined as the sum of all incoming and outgoing connections per node. Strength is derived as the total weight of all incoming and outgoing connections per node. Betweenness expresses the fraction of shortest paths that pass through each node. Closeness is calculated as the average of the row and column sum of the network's distance matrix (the out-closeness), which represents a matrix of the lengths of the shortest paths between all node pairs. The distance matrix is derived from the weighted connection matrix, after converting connection weights to lengths using the inverse transform.

After computing these four centrality measures, nodes were ranked on each of the four metrics, and an aggregate "hub score" was determined for each node, expressing the number of metrics for which each node appeared in the top 10% (top 7). For example, a node that achieved a top 10% ranking in all four centrality metrics was given a score of 4. Data on all four centrality measures are shown in Fig. S1*C*, and aggregate hub scores for hubs are given in Fig. S2 (highlighted in red).

Rich-club analysis proceeded along the lines of previous studies carried out in weighted networks (22). Rich-club organization is present if high-degree nodes of a network are more densely connected among themselves than expected by chance (23). In general, rich-club organization is detected by comparing connection weight among nodes with minimum degree $k$ to the equivalent weight in a population of randomized networks. Analysis proceeds along these steps. For each value of $k$, the total sum of the weights $W_{>k}$ between all nodes with degree $k$ or higher was determined. No distinction is made between incoming or outgoing connection weights. Next, the weighted rich-club coefficient $\Phi^w(k)$ was computed as the ratio between $W_{>k}$ and the sum of the weights of the strongest $E_{>k}$ connections across the whole network. The weighted rich-club coefficient was then normalized against a set of 10,000 randomly rewired networks, preserving network size, weight, and degree sequence (see above). Comparison of the rich-club coefficient of the empirical network to this random null distribution was then subjected to significance testing. To correct for multiple comparisons over the range of degrees $k$ examined, false-discovery rate correction was performed (24), at a false-discovery rate of 0.001.

Connection patterns were statistically analyzed by comparing the empirical connection matrix to a random population of networks with an identical adjacency matrix (that is, no rewiring of connections) but with randomly permuted connection weights on existing connections. Only connections linking node pairs for which connection weights had been empirically established in both directions were considered in this analysis. Permutation of weights was carried out 100,000 times. The connection weight matrices were organized by weight class (very weak, weak, weak/moderate, moderate, moderate/strong, strong, and very strong).

Patterns of intramodular and intermodular connections were investigated by counting the number of connections for each weight class and for each intramodular or intermodular block of the connection matrix (Tables S1 and S2 and Fig. 2). Additional analyses were carried out on a modified version of the original weighted connection matrix that comprised only connections of at least weak/moderate weight, called major connections (very weak, weak, and exists connection weights, $n = 442$, were set to zero for this analysis because they most likely contribute to false positive results; for the remaining, $n = 1{,}481$). Applying the module partition depicted in Fig. 2 to this network yielded weight distributions for unidirectional connections within and between module blocks (Table S3). Comparison with weight distributions in the random null model allowed z-score calculations to identify significant differences.

RCAMs within and between P1 and P3 were analyzed by dividing connection weights into three categories: major (very strong and strong), medium (moderate/strong to weak/moderate), and minor (weak and very weak). The number of RCAMs in each category, within and between poles, is shown in Tables S4 and S5. In addition, possible asymmetries in RCAMs between poles were evaluated as ratios of the percentages of bidirectional macroconnections in each weight category (Tables S4 and S5). If the percentage of connections from–to and to–from is equal, the asymmetry is 0; if the ratio is 6:1, asymmetry is 5.

The impact of dataset completeness on module configuration was examined in two ways. First, the final dataset representing 81% coverage (matrix fill ratio) of all possible cortical association connections was compared with eight earlier compilations, representing 22%, 35%, 52%, 56%, 60%, 65%, 73%, and 78% coverage (Fig. 8). Second, the final dataset was randomly pruned by deleting a randomly and uniformly selected fraction of connections. This process, which resulted in a gradual thinning out of the connection matrix from 81% coverage down to 22% coverage, was carried out a total of 100 times. At each level of network coverage (fill ratio), network modules were derived as described above (10,000 runs of the Louvain algorithm). Similarity between the optimal module partition (Fig. 2) for 81% fill ratio and partitions for networks with lower fill ratios was assessed by plotting the number of modules (Fig. 8) as well as the similarity (Pearson correlation) of the network's agreement matrices (Fig. 8*C*). For a given network, the agreement matrix was computed by aggregating all module partitions across 10,000 runs, expressing for each node pair the proportion of times the node pair was assigned to the same module. The similarity measure plotted in Fig. 8*C* was computed as the Pearson correlation between the upper triangle of the agreement matrix of the 81% fill ratio network and the upper triangle of the agreement matrix of the degraded or incompletely filled matrices.


1. Swanson LW (2004) *Brain Maps: Structure of the Rat Brain. A Laboratory Guide with Printed and Electronic Templates for Data, Models and Schematics* (Elsevier, Amsterdam), 3rd Ed.
2. International Commission on Zoological Nomenclature (1999) *International Code of Zoological Nomenclature* (International Trust for Zoological Nomenclature, London).
3. Cenquizca LA, Swanson LW (2007) Spatial organization of direct hippocampal field CA1 axonal projections to the rest of the cerebral cortex. *Brain Res Brain Res Rev* 56(1):1–26.
4. Bota M, Dong H-W, Swanson LW (2012) Combining collation and annotation efforts toward completion of the rat and mouse connectomes in BAMS. *Front Neuroinform* 6:2.
5. Bota M, Talpalaru S, Hintiryan H, Dong H-W, Swanson LW (2014) BAMS2 workspace: A comprehensive and versatile neuroinformatic platform for collating and processing neuroanatomical connections. *J Comp Neurol* 522(14):3160–3176.
6. Bota M, Dong H-W, Swanson LW (2003) From gene networks to brain networks. *Nat Neurosci* 6(8):795–799.
7. Swanson LW, Bota M (2010) Foundational model of structural connectivity in the nervous system with a schema for wiring diagrams, connectome, and basic plan architecture. *Proc Natl Acad Sci USA* 107(48):20610–20617.
8. de Reus MA, van den Heuvel MP (2013) Rich club organization and intermodule communication in the cat connectome. *J Neurosci* 33(32):12929–12939.
9. Zingg B, et al. (2014) Neural networks of the mouse neocortex. *Cell* 156(5):1096–1111.
10. Stephan KE, et al. (2001) Advanced database methodology for the Collation of Connectivity data on the Macaque brain (CoCoMac). *Philos Trans R Soc Lond B Biol Sci* 356(1412):1159–1186.
11. Hahn JD, Swanson LW (2012) Connections of the lateral hypothalamic area juxtadorsomedial region in the male rat. *J Comp Neurol* 520(9):1831–1890.
12. Markov NT, et al. (2014) A weighted and directed interareal connectivity matrix for macaque cerebral cortex. *Cereb Cortex* 24(1):17–36.
13. Gabbott PL, Warner TA, Jays PR, Salway P, Busby SJ (2005) Prefrontal cortex in the rat: Projections to subcortical autonomic, motor, and limbic centers. *J Comp Neurol* 492(2):145–177.
14. Kerr KM, Agster KL, Furtak SC, Burwell RD (2007) Functional neuroanatomy of the parahippocampal region: The lateral and medial entorhinal areas. *Hippocampus* 17(9):697–708.
15. Sanderson KJ, Dreher B, Gayer N (1991) Prosencephalic connections of striate and extrastriate areas of rat visual cortex. *Exp Brain Res* 85(2):324–334.

16. Boss BD, Turlejski K, Stanfield BB, Cowan WM (1987) On the numbers of neurons in fields CA1 and CA3 of the hippocampus of Sprague-Dawley and Wistar rats. *Brain Res* 406(1-2):280–287.
17. Rubinov M, Sporns O (2010) Complex network measures of brain connectivity: Uses and interpretations. *Neuroimage* 52(3):1059–1069.
18. Blondel V, Guillaume JL, Lambiotte R, Lefebvre E (2008) Fast unfolding of communities in large networks. *J Stat Mech* P10008.
19. Newman MEJ, Girvan M (2004) Finding and evaluating community structure in networks. *Phys Rev E Stat Nonlin Soft Matter Phys* 69(2 Pt 2):026113.
20. Bullmore E, Sporns O (2009) Complex brain networks: Graph theoretical analysis of structural and functional systems. *Nat Rev Neurosci* 10(3):186–198.
21. Maslov S, Sneppen K (2002) Specificity and stability in topology of protein networks. *Science* 296(5569):910–913.
22. van den Heuvel MP, Sporns O (2011) Rich-club organization of the human connectome. *J Neurosci* 31(44):15775–15786.
23. Colizza V, Flammini A, Serrano MA, Vespignani A (2006) Detecting rich-club ordering in complex networks. *Nat Phys* 2:110–115.
24. Benjamini Y, Hochberg Y (1995) Controlling the false discovery rate: A practical and powerful approach to multiple testing. *J R Stat Soc, B* 57:289–300.

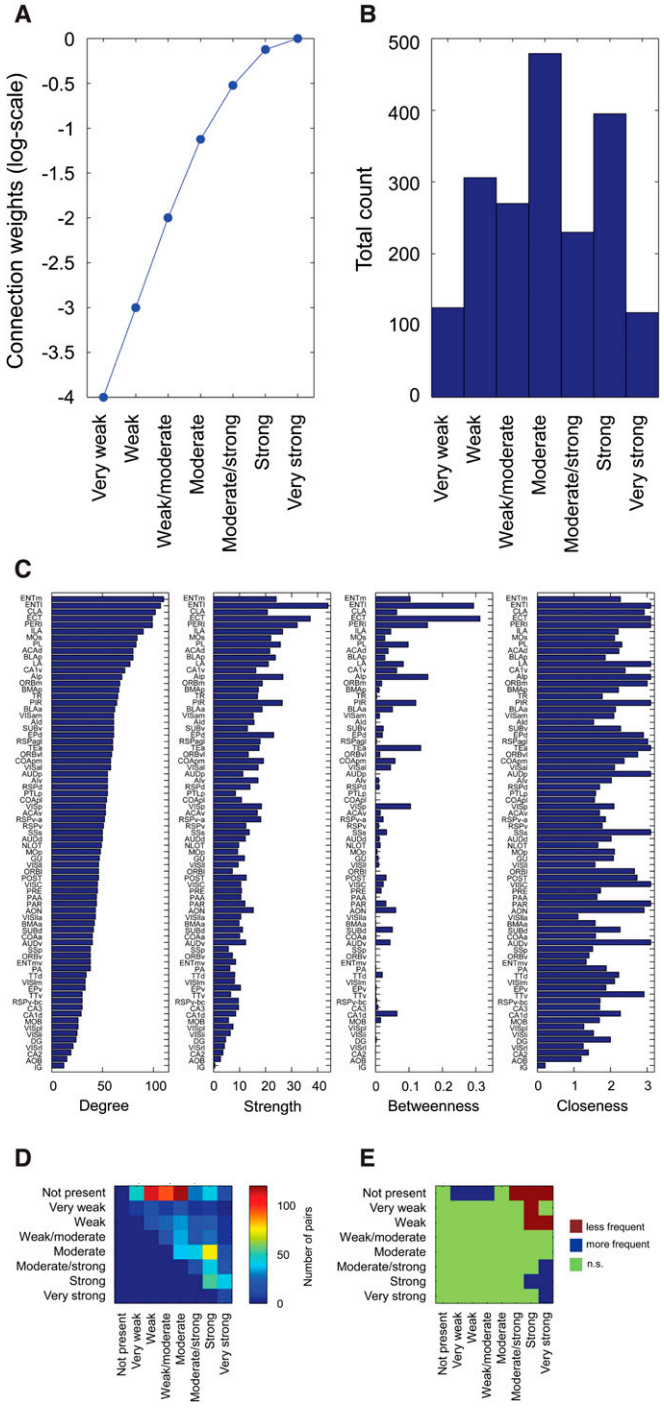


**Fig. S1.** Network analysis features. (*A* and *B*) Connection weight scaling and distribution with log-transformed connection weights for each of eight weight categories on an ordinal scale (*A*) and histogram of weight classes across the network (*B*). (*C*) Centrality and hubs with node degree for all 73 rat cortical regions, displayed in order of degree, from top to bottom on the left. This node ordering is maintained across all remaining plots in this figure, including node strength, betweenness, and closeness, as indicated at the bottom. (*D* and *E*) Weight class pairing frequencies for all bidirectional association connections. In *D*, only node pairs for which data on connections in both directions (including data on absence of a connection) has been obtained are considered. Each entry in the matrix represents a count of the number of bidirectional connections for which the two weight classes are paired. For example, the most frequent combination is "one connection absent" and "one connection moderate." Only the main diagonal and upper triangle of the matrix are considered because of symmetry. *E* shows significant positions in matrix (*D*), after comparison with a random null model. Blue ("more frequent") refers to combinations of weights that are more frequent in the empirical matrix ($P < 0.0014$, Bonferroni corrected), and red ("less frequent") refers to combinations that are more frequent in the null model ($P > 0.0014$, Bonferroni corrected), and green ("n.s.") refers to combinations that do not differ significantly. This analysis indicates that highly asymmetric weight combinations are less frequently encountered in the empirical connection matrix than expected if weights were randomly assigned to existing connections.

| | Rat | Human |
|---|---|---|
| Module 1 (M1, N = 15) (Caudal hemispheric or caudal core module) | Ventral auditory areas (AUDv) | Within parainsular (52) and lateral (posterior) transverse temporal (42) areas; belt primary auditory cortex* |
| | Primary auditory area (AUDp) | Medial (anterior) transverse temporal area (41); core primary auditory cortex* |
| | Dorsal auditory areas (AUDd) | Within parainsular (52) and lateral (posterior) transverse temporal (42) areas; belt primary auditory cortex* |
| | Temporal association areas (TEa) [dorsal] [2] | Inferior temporal (20), middle temporal (21), superior temporal (22), occipitotemporal (37), temporopolar (38) areas |
| | Ectorhinal area (ECT) [ventral temporal association] [4] | Ectorhinal area (36) |
| | Laterolateral visual area (VISll) | Within occipital (18) and preoccipital (19) areas |
| | Anterior laterolatertal visual area (VISlla) | Within occipital (18) and preoccipital (19) areas |
| | Intermediolateral visual area (VISli) | Within occipital (18) and preoccipital (19) areas |
| | Primary visual area (VISp) [1] | Striate area (17) |
| | Anterolateral visual area (VISal) | Within occipital (18) and preoccipital (19) areas |
| | Posterolateral visual area (VISpl) | Within occipital (18) and preoccipital (19) areas |
| | Anteromedial visual area (VISam) | Within occipital (18) and preoccipital (19) areas |
| | Mediolateral visual area (VISlm) | Within occipital (18) and preoccipital (19) areas |
| | Rostrolateral visual area (VISrl) | Within occipital (18) and preoccipital (19) areas |
| | Parietal region, posterior association areas (PTLp) | Preparietal (5), superior parietal (7), angular (39), and supramarginal (40) areas |
| Module 2 (M2, N = 15) (Rostral hemispheric or rostral core module) | Primary somatosensory area (SSp) | Intermediate, caudal, rostral postcentral areas (1, 2, 3) |
| | Supplemental somatosensory area (SSs) | Roughly subcentral area (43); secondary & ventral parietal somatosensory areas* |
| | Visceral area (VISC) | Part of posterior granular zone, insular region (areas 13-16) |
| | Gustatory area (GU) | Part of posterior granular zone, insular region (areas 13-16) |
| | Agranular insular area, posterior part (AIp) [3] | Part of anterior agranular zone, insular region (areas 13-16) |
| | Perirhinal area (PERI) [4] | Perirhinal area (35) |
| | Agranular insular area, dorsal part (AId) | Part of anterior agranular zone, insular region (areas 13-16) |
| | Primary somatomotor area (MOp) | Giant pyramical area (4); primary somatomotor area* |
| | *Basolateral amygdalar nucleus, anterior part (BLAa)* | *Brodmann did not recognize; part of basolateral amygdalar complex (BLC)*** |
| | Secondary somatomotor areas (MOs) [1] | Agranular (6) intermediate (8), granular (9), frontopolar (10), opercular (44), triangular (45), middle (46) frontal areas |
| | *Claustrum (CLA)* [1] | *Brodmann did not recognize; claustrum** |
| | Orbital area, ventrolateral part (ORBvl) | Part of prefrontal area (11); see** |
| | Orbital area, medial part (ORBm) | Part of prefrontal area (11); see** |
| | Orbital area, ventral part (ORBv) | Part of prefrontal area (11); see** |
| | Orbital area, lateral part (ORBl) | Roughly orbital area (47); see** |
| Module 3 (M3, N = 16) (Dorsal limbic or dorsal shell module) | Anterior cingulate area, dorsal part (ACAd) | Part of cingulate region (mainly areas 31, 32)* |
| | Retrosplenial area, ventral part, zone b/c (RSPv-b/c) | Part of granular retrolimbic area (29)* |
| | Anterior cingulate area, ventral part (ACAv) | Part of cingulate region (mainly areas 23, 24)* |
| | Retrosplenial area, dorsal part (RSPd) | Part of agranular retrolimbic area (30)* |
| | Retrosplenial area, ventral part (RSPv) | Part of granular retrolimbic area (29)* |
| | Retrosplenial area, lateral agranular part (RSPagl) | Part of agranular retrolimbic area (30)* |
| | Retrosplenial area, ventral part, zone a (RSPv-a) | Part of granular retrolimbic area (29)* |
| | Postsubiculum (POST) | Retrosubicular area (48); postsubiculum** |
| | Subiculum, dorsal zone (SUBd) | Brodmann did not recognize; subiculum, dorsal zone** |
| | Presubiculum (PRE) | Presubicular area (27); presubiculum** |
| | Parasubiculum (PAR) | Parasubicular area (49); parasubiculum** |
| | Entorhinal area, medial part (ENTm) [1] | Entorhinal area (28); medial part** |
| | Field CA3, Ammon's horn (CA3) | Brodmann did not recognize; field CA3, Ammon's horn** |
| | Field CA1, Ammon's horn, dorsal subregion (CA1d) | Brodmann did not recognize; field CA1, Ammon's horn, dorsal zone** |
| | Field CA2, Ammon's horn (CA2) | Brodmann did not recognize; field CA2** |
| | Dentate gyrus (DG) | Brodmann did not recognize; dentate gyrus** |
| Module 4 (M4, N = 27) (Ventral limbic or ventral shell module) | Induseum griseum (IG) | Dorsal part of pregenual area (33); induseum griseum* |
| | Accessory olfactory bulb (AOB) | [Not present in adult human] |
| | Main olfactory bulb (MOB) | Olfactory bulb |
| | Tenia tecta, ventral part (TTv) | Ventral part of pregenual area (33); tenia tecta (TT)* |
| | Anterior olfactory nucleus (AON) | Olfactory peduncle** |
| | Tenia tecta, dorsal part (TTd) | Ventral part of pregenual area (33); tenia tecta (TT)* |
| | Nucleus of lateral olfactory tract (NLOT) | Part of amygdaloid nucleus (AA); part of cortical amygdalar complex (CAC)** |
| | Piriform area (PIR) [3] | Prepyriform area (51) |
| | Cortical amygdalar nucleus, anterior part (COAa) | Part of amygdaloid nucleus (AA); part of cortical amygdalar complex (CAC)** |
| | *Basomedial amydgalar nucleus, anterior part (BMAa)* | *Brodmann did not recognize; part of basolateral amygdalar complex (BLC)*** |
| | Agranular insular area, ventral part (AIv) | Ventral part of anterior agranular zone, insular region (areas 13-16) |
| | *Endopiriform nucleus, dorsal part (EPd)* | *Brodmann did not recognize; deep dorsal part of area 51* |
| | Piriform-amygdalar area (PAA) | Part of amygdaloid nucleus (AA); part of cortical amygdalar complex (CAC)** |
| | *Endopiriform nucleus, ventral part (EPv)* | *Brodmann did not recognize; deep ventral part of area 51* |
| | Cortical amydgalar nuclues, posteromedial part (COApm) | Part of amygdaloid nucleus (AA); part of cortical amygdalar complex (CAC)** |
| | Entorhinal area, lateral part (ENTl) [4] | Entorhinal area (28); lateral part** |
| | Cortical amygdalar nucleus, posterolateral part (COApl) | Part of amygdaloid nucleus (AA); part of cortical amygdalar complex (CAC)** |
| | Postpiriform transition area (TR) | Part of amygdaloid nucleus (AA); part of cortical amygdalar complex (CAC)** |
| | Infralimbic area (ILA) [2] | At least part of subgenual area (25)** |
| | *Basolateral amygdalar nucleus, posterior part (BLAp)* | *Brodmann did not recognize; part of basolateral amygdalar complex (BLC)*** |
| | *Basomedial amygdalar nucleus, posterior part (BMAp)* | *Brodmann did not recognize; part of basolateral amygdalar complex (BLC)*** |
| | Prelimbic area (PL) [1] | Probably dorsal part of subgenual area (25) |
| | *Lateral amygdalar nucleus (LA)* [1] | *Brodmann did not recognize; part of basolateral amygdalar complex (BLC)*** |
| | Field CA1, Ammon's horn, ventral subregion (CA1v) | Brodmann did not recognize; field CA1, Ammon's horn, ventral zone** |
| | Subiculum, ventral zone (SUBv) | Brodmann did not recognize; subiculum, ventral zone** |
| | *Posterior amygdalar nucleus (PA)* | *Brodmann did not recognize; part of basolateral amygdalar complex (BLC)*** |
| | Entorhinal area, medial part, ventral zone (ENTmv) | Entorhinal area (28); medial part, ventral zone** |

**Fig. S2.** Module composition. The left column shows regional composition of the four rat cortical association connection modules (Figs. 2–7). Regions highlighted in red had the highest aggregate score on four centrality measures (with the score shown in brackets; Fig. S1*C*). The three cortical regions with the highest aggregate score value (a value of 4) are considered network hubs. The right column shows proposed general correspondence between adult rat and human cerebral cortical regions based on a preponderance of current evidence. Documentation for this working hypothesis is based on Swanson (1) for rat and Brodmann (2) and others, indicated by asterisks, for human. Brodmann's (2) overall scheme for mammals (based on 64 species in 7 orders) has been confirmed, although many areas have been further subdivided and/or renamed, and some important boundary controversies remain unresolved. There is no modern experimental axonal pathway tracing data for human association cortical connections; proposed correspondence of gray-matter regions is based on cellular architecture, topological relationships, and functional studies. Parts of the cortical subplate are italicized. *n*, number of gray matter regions within a module. *, see ref. 3; **, see ref. 4.

1. Swanson LW (2004) *Brain Maps: Structure of the Rat Brain. A Laboratory Guide with Printed and Electronic Templates for Data, Models and Schematics* (Elsevier, Amsterdam), 3rd Ed.

2. Brodmann K (2006) *Brodmann's Localization in the Cerebral Cortex: The Principles of Comparative Localisation in the Cerebral Cortex Based on the Cytoarchitectonics*; trans Garey L (Springer, New York).
3. Nieuwenhuys R, Voogd J, van Huijzen C (2008) *The Human Central Nervous System* (Springer, Berlin), 4th Ed.
4. Swanson LW (2014) *Neuroanatomical Terminology: A Lexicon of Classical Origins and Historical Foundations* (Oxford Univ Press, New York).

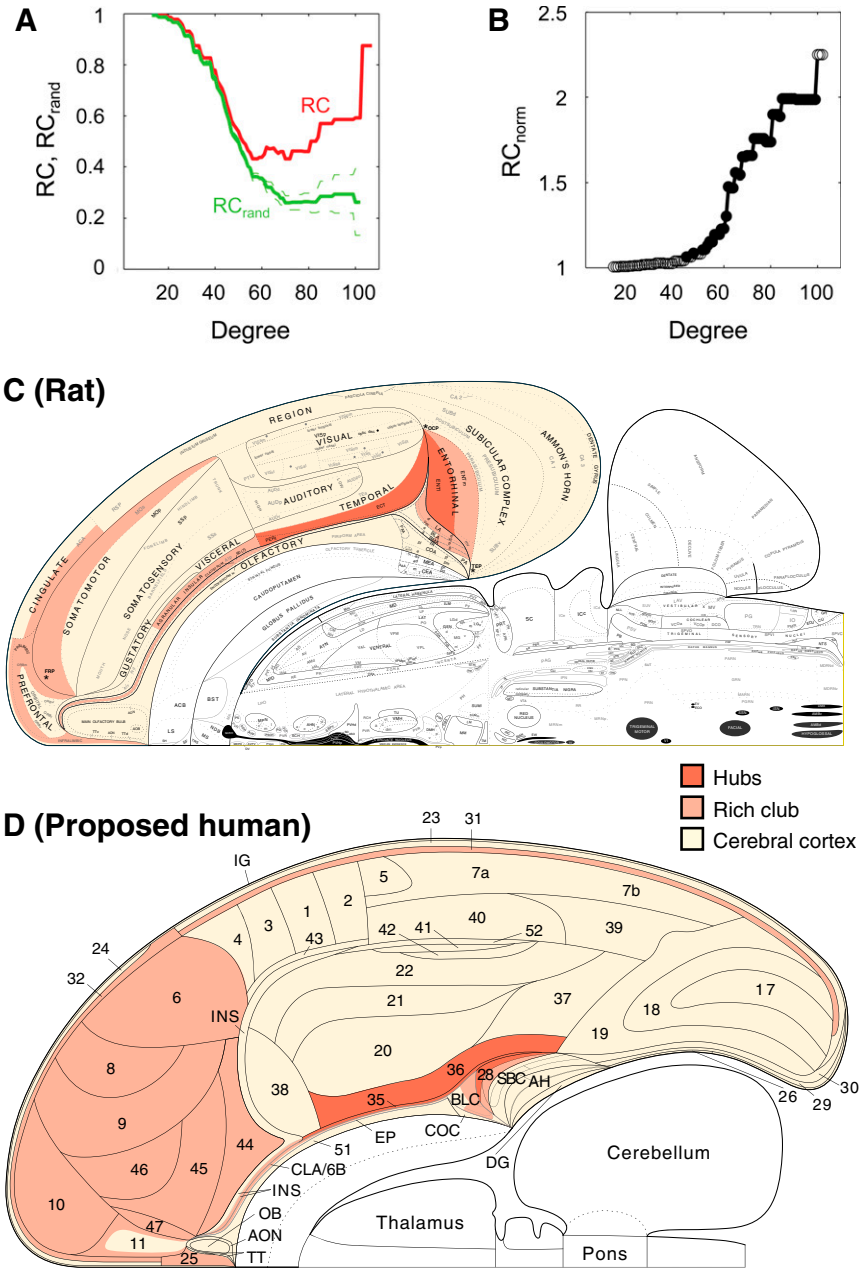


**Fig. S3.** Rich-club coefficients and their anatomical distribution with hubs. (*A*) Curves for the weighted rich-club coefficient of the empirical network (*RC*, solid red) and the mean ($RC_{rand}$, solid green) and SD (stippled green) values for the corresponding random null model. (*B*) Normalized rich-club coefficient as a function of minimum degree *k*. Levels at which the normalized coefficient was significantly different from the null distribution (at a false discovery rate of $P < 0.001$) are indicated by filled symbols. (*C* and *D*) Rich club and hubs plotted on flatmaps of the rat (*C*) and human (*D*) central nervous system (right half) as in Fig. 4 *A* and *C*. The lateral entorhinal area (ENTl) is unique insofar as it is a member of both the set of three highest ranked hubs and the set of three members of the innermost circle of rich-club nodes; it is especially implicated in the earliest stages of Alzheimer's disease (1). Proposed correspondence between rat and human cortical regions as in Fig. S2 (where abbreviations are provided).

1. Braak H, Rüb U, Schultz C, Del Tredici K (2006) Vulnerability of cortical neurons to Alzheimer's and Parkinson's diseases. *J Alzheimers Dis* 9(3, Suppl)35–44.

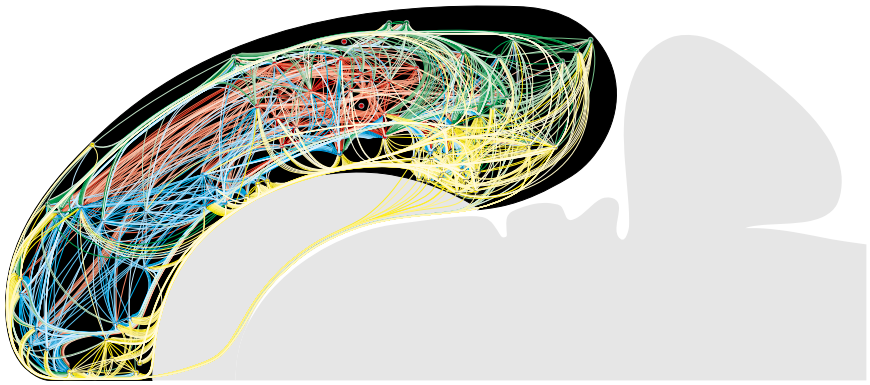

**Fig. S4.** RCAM displayed on flatmap, same as Fig. 6, but with higher resolution and labeled nodes. The file was created in Adobe Illustrator (Version 16.0.0), where data layering is available. Abbreviations are as in Fig. S2.

**Table S1. Connection weight distributions within and between modules by weight and module: Connection qualitative strengths, counts**

| | Very strong | Strong | Moderate/strong | Moderate | Weak/moderate | Weak | Very weak |
|---|---|---|---|---|---|---|---|
| M1->M1 | 15 | 57 | 19 | 40 | 11 | 7 | 1 |
| M1->M2 | 2 | 12 | 17 | 19 | 19 | 21 | 3 |
| M1->M3 | 1 | 4 | 6 | 21 | 21 | 12 | 9 |
| M1->M4 | 2 | 4 | 21 | 10 | 5 | 6 | 5 |
| M2->M1 | 6 | 3 | 11 | 21 | 21 | 16 | 8 |
| M2->M2 | 15 | 40 | 22 | 44 | 26 | 13 | 2 |
| M2->M3 | 1 | 8 | 5 | 22 | 16 | 12 | 13 |
| M2->M4 | 11 | 27 | 15 | 33 | 19 | 25 | 9 |
| M3->M1 | 1 | 3 | 9 | 26 | 14 | 18 | 6 |
| M3->M2 | 2 | 9 | 5 | 6 | 8 | 11 | 13 |
| M3->M3 | 19 | 50 | 19 | 25 | 10 | 21 | 4 |
| M3->M4 | 3 | 11 | 5 | 21 | 15 | 19 | 8 |
| M4->M1 | 1 | 4 | 6 | 4 | 6 | 16 | 18 |
| M4->M2 | 7 | 20 | 17 | 43 | 24 | 21 | 7 |
| M4->M3 | 4 | 16 | 11 | 20 | 13 | 26 | 9 |
| M4->M4 | 28 | 116 | 60 | 124 | 42 | 62 | 10 |

Number of rat macroconnections by connection weight and cortical association module (M1–M4), given as absolute values (counts).

**Table S2. Connection weight distributions within and between modules by weight and module: Connection qualitative strengths, percentages**

| | Very strong, % | Strong, % | Moderate/strong, % | Moderate, % | Weak/moderate, % | Weak, % | Very weak, % |
|---|---|---|---|---|---|---|---|
| M1->M1 | 10 | 38 | 13 | 27 | 7 | 5 | 1 |
| M1->M2 | 2 | 13 | 18 | 20 | 20 | 23 | 3 |
| M1->M3 | 1 | 5 | 8 | 28 | 28 | 16 | 12 |
| M1->M4 | 4 | 8 | 40 | 19 | 9 | 11 | 9 |
| M2->M1 | 7 | 3 | 13 | 24 | 24 | 19 | 9 |
| M2->M2 | 9 | 25 | 14 | 27 | 16 | 8 | 1 |
| M2->M3 | 1 | 10 | 6 | 29 | 21 | 16 | 17 |
| M2->M4 | 8 | 19 | 11 | 24 | 14 | 18 | 6 |
| M3->M1 | 1 | 4 | 12 | 34 | 18 | 23 | 8 |
| M3->M2 | 4 | 17 | 9 | 11 | 15 | 20 | 24 |
| M3->M3 | 13 | 34 | 13 | 17 | 7 | 14 | 3 |
| M3->M4 | 4 | 13 | 6 | 26 | 18 | 23 | 10 |
| M4->M1 | 2 | 7 | 11 | 7 | 11 | 29 | 33 |
| M4->M2 | 5 | 14 | 12 | 31 | 17 | 15 | 5 |
| M4->M3 | 4 | 16 | 11 | 20 | 13 | 26 | 9 |
| M4->M4 | 6 | 26 | 14 | 28 | 10 | 14 | 2 |

Number of rat macroconnections by connection weight and cortical association module (M1–M4), given as percentages.

**Table S3. Major unidirectional connections within and between modules**

| | Major unidirectional RCAMs (from very strong to weak/moderate) | | | | | | | |
|---|---|---|---|---|---|---|---|---|
| | M1-> | | M2-> | | M3-> | | M4-> | |
| | Absolute nos. (counts) | Percentages, % | Absolute nos. (counts) | Percentages, % | Absolute nos. (counts) | Percentages, % | Absolute nos. (counts) | Percentages, % |
| M1 | 142* | 49* | 62 | 16 | 53 | 20 | 21** | 4** |
| M2 | 69 | 24 | 147* | 41* | 30** | 11** | 111 | 20 |
| M3 | 53 | 18 | 52 | 14 | 123* | 47* | 64** | 11** |
| M4 | 24** | 8** | 105 | 29 | 55** | 21** | 370* | 65* |

RCAMs within and between modules (M1–M4) are given as absolute values (counts) and as percentages. Statistically significant values are indicated with asterisks. Major connections include weights very strong through weak/moderate. *$z > 5$; **$z \leq 5$.

**Table S4. Connections within and between rich-club poles**

| | P1 | | P2 | | P3 | |
|---|---|---|---|---|---|---|
| Poles | Counts | Percentages, % | Counts | Percentages, % | Counts | Percentages, % |
| Major (very strong and strong) connections | | | | | | |
| P1 | 12 | 67 | 4 | 20 | 13 | 68 |
| P2 | 9 | 39 | 10 | 50 | 10 | 71 |
| P3 | 6 | 35 | 3 | 18 | 4 | 33 |
| Medium (strong/moderate, moderate, and moderate/weak) connections | | | | | | |
| P1 | 6 | 33 | 13 | 65 | 6 | 32 |
| P2 | 8 | 35 | 9 | 45 | 4 | 29 |
| P3 | 9 | 53 | 13 | 76 | 4 | 33 |
| Minor (weak and very weak) connections | | | | | | |
| P1 | 0 | 0 | 3 | 15 | 0 | 0 |
| P2 | 6 | 26 | 1 | 5 | 0 | 0 |
| P3 | 2 | 12 | 1 | 6 | 4 | 33 |
| Total connections | | | | | | |
| P1 | 18 | | 20 | | 19 | |
| P2 | 23 | | 20 | | 14 | |
| P3 | 17 | | 17 | | 12 | |

The distribution of rat macroconnection weight categories by rich-club poles (P1–P3; see text). Number of macroconnections in each category is given separately as an absolute count and as a percentage.

**Table S5. Asymmetries between rich-club poles**

| | Asymmetries between poles | | | | | |
|---|---|---|---|---|---|---|
| | Difference between pole connections (counts) by categories | | | Asymmetry by connection category | | |
| | Major | Medium | Minor | Major | Medium | Minor |
| P1 -> P2 | 9 | 8 | 6 | 1.25 | 0.63 | 1 |
| P2 -> P1 | 4 | 13 | 3 | | | |
| P1 -> P3 | 6 | 9 | 2 | 1.17 | 0.5 | 2 |
| P3 -> P1 | 13 | 6 | 0 | | | |
| P2 -> P3 | 3 | 13 | 1 | 2.33 | 2.25 | 1 |
| P3 -> P2 | 10 | 4 | 0 | | | |

The distribution of rat macroconnection weight categories by rich-club poles (P1–P3; see text), and asymmetry values for each pair of poles.

**Table S6. Degree of coverage (fill ratio) of intramodular and intermodular connection matrices**

| | Coverage degrees of intra- and intermodular connection matrices, % | | | |
|---|---|---|---|---|
| | M1 | M2 | M3 | M4 |
| M1 | 85.2 | 85.2 | 77.2 | 84.1 |
| M2 | 89.1 | 91.9 | 86.2 | 92.6 |
| M3 | 76.9 | 85.8 | 85.8 | 80.7 |
| M4 | 78.2 | 89.2 | 71.9 | 88.9 |

Values are percent coverage of macroconnection data for indicated matrices.

**Table S7. Comparison of present cerebral cortex analysis in rat with two recent analyses in mouse**

| Source | Total gray matter regions* | Pathway tracer direction | Axon terminals (1) analyzed | Network type | Network directionality |
|---|---|---|---|---|---|
| Zingg et al., 2014 (2) | 37[†] | Anterograde and retrograde | Yes | Binary | Yes |
| Oh et al., 2014 (3) | 19[c‡] | Anterograde | No[§] | Binary | No[¶] |
| Present work | 73[‖] | Anterograde and retrograde | Yes | Weighted | Yes |

*With anterograde and/or retrograde pathway tracer injection site confined to region of interest (anterograde to region of pathway origin, retrograde to region of pathway termination); that is, with no significant pathway tracer injection site labeling of adjacent (secondary) regions. All three studies used virtually the same cortical nomenclature (gray matter region parts list) for rodents.

[†]Regions are 31 isocortex, 3 olfactory cortex, 2 hippocampal formation, and 1 subplate (Figure 2*E* in ref. 2).

[‡]Regions are 12 isocortex, 2 olfactory cortex, 5 hippocampal formation, and 0 subplate. Figure 4 in ref. 3 shows many regions where the injection site spread to include major extents of nearby regions (not indicated here but listed in Supplemental Table 2 in ref. 3) and thus seriously confounding interpretation of the connectional results. Supplemental Table 2 in ref. 3 lists 19 cortical regions where the injection site was confined or nearly confined to the region of interest.

[§]Fibers (axons) and axon terminals measured together, not distinguished.

[¶]Figure 4 in ref. 3 shows a directional matrix, but network analysis was performed on a binary and nondirectional matrix (Supplementary Information in ref. 3).

[‖]All cortical plate and subplate gray matter regions except two, the tiny and obscure fasciola cinerea (cortical plate) and sublayer 6b (cortical subplate).

1. Swanson LW, Bota M (2010) Foundational model of structural connectivity in the nervous system with a schema for wiring diagrams, connectome, and basic plan architecture. *Proc Natl Acad Sci USA* 107(48):20610–20617.
2. Zingg B, et al. (2014) Neural networks of the mouse neocortex. *Cell* 156(5):1096–1111.
3. Oh SW, et al. (2014) A mesoscale connectome of the mouse brain. *Nature* 508(7495):207–214.